IN THE NAME OF

ALLAH

THE MOST BENEFICENT

THE MOST MERCIFUL

CONSTRUCTION AND CALIBRATION OF LOW TEMPERATURE THERMAL CONDUCTIVITY MEASUREMENT APPARATUS

A dissertation submitted to the Department of Physics, Quaid-i-Azam University, Islamabad, in the partial fulfillment of the requirement for the degree of

MASTER OF PHILOSOPHY

in

PHYSICS

by

MUHAMMAD ARSHAD

DEPARTMENT OF PHYSICS
QUAID-I-AZAM UNIVERSITY
ISLAMABAD

1994

CERTIFICATE

Certified that the experimental work in this dissertation has been carried out by **Mr. Muhammad Arshad** under my supervision and is accepted in its present form by the Department of Physics, Quaid-i-Azam University, Islamabad, as satisfying the dissertation requirement for the degree of **Master of Philosophy in Physics.**

Prof. Dr. Asghari Maqsood
Supervisor
Department of Physics
Quaid-i-Azam University
Islamabad.

Submitted through

Prof. Dr. Kamaluddin Ahmed
Chairman
Department of Physics
Quaid-i-Azam University
Islamabad.

DEDICATED

to the grieved memories of my

(LATE) MOTHER

who bereaved me at my early teething stage and, unfortunately, I don't even have any fond memory about her to boast of:

With her I take delight in weal,
And seek relief in woe;
But while I understand and feel
How much to her I owe
My cheeks have often been bedew'd
with tears of thoughtful gratitude
What have I done, or tried, or said
In thanks to that dear mother dead ?
What have I done to keep in mind
My debt to her and mankind ?

ACKNOWLEDGMENTS

All commendations to Almighty Allah, Who imparted me resoluteness and fortitude for the accomplishment of this scientific assignment. I offer my humblest and sincerest words of thanks to His Holy Prophet Mohammed (Peace be upon him) who is forever a torch of guidance and knowledge for humanity.

I consider myself fortune to be a member of a research group where an atmosphere of cooperative spirit and mutual support prevails. Each and every member of the Thermal Physics group owes my gratitude for discussing my work with me and easing my frustrating moments with some laughs and a cup of tea.

Needless to say about the distinguished supervisor, Prof. Dr. Asghari Maqsood who has played the most important and pivotal role during my academic journey. Her painstaking supervision and challenging queries were indispensable to my research work. She has been much more than supervisor. so again my sincere thanks for the guidence, inspiration and unabated vigor to her and to her family for kindness during the whole period of my study.

Mr. Izhar ul-haq and Mr. M. Maqsood have given me the benefit of their insight and incisive opinion during the early stages of writing with unfailing encouragement and support over the entire timings of my research work. Their comments and suggestions resulted in substantial improvements in the experimental work. Mr. M. Maqsood read the manuscript with admirable competence but always went through the innumerable revisions with patience, care and understanding. My sincerest thanks are due to these senior research scholars.

My special thanks are due to Miss Zahida Ali whose help and cooperation was of great importance to my work. The responsibility for any remaining errors or shortcomings is, of course mine.

I am also very grateful to the Chairman Department of Physics for the provision of all possible facilities.

I am grateful to Prof. Dr. Farid Ahmad Khawaja, of Materials Science Laboratory for useful discussions and fine critical comments on the text of this thesis.

I would like to acknowledge the University Grants Commission Islamabad Pakistan, for providing me the Research Scholarship during my M. Phil. studies.

My thanks are due to the lab assistant M. Ismail for technical help and taking care of the work related to the maintenance of the Thermal Physics Lab.

I would like to express my deep appreciation for my teachers, colleagues at department and friends specially Mr. S. Imtiaz Karim (SAARC scholar at NIP), Mr. Shahid Ali Shah , Mr. Maqsood Ahmad, good times we have spent together and for all those who helped me through the long and trying hours of my life.

Finally, I owe my profoundest gratitude's to my parents for their mellifluous affections and all the family members particularly, my uncle Mohammad Hanif for remembering me in their prayers which hearten me to achieve success in every sphere of life and encouraged me throughout the span of study.

MOHAMMAD ARSHAD

ABSTRACT

Comprehensive effort has been ensued in the construction and calibration of thermal conductivity measurement apparatus implementing the latest developed transient plane source (TPS) technique. The technique is also used to probe some critical physical phenomenon, such as the enhancement of thermal conductivity of high-T_c superconductors in the superconducting state. A " resistive element ", the TPS-element, is used both as heat source and as temperature sensor. Measurements on fused quartz as a standard sample were performed for calibration purpose and to demonstrate that this experimental setup using this technique can be used down to liquid nitrogen temperature. A simple low temperature arrangement was installed and used with vacuum system containing rotary pump for vacuum purposes. The results of our data are within an error of 2% found in agreement with the standard curve in the literature. Then a carbon steel sample and a sintered superconductor, sample were studied for the thermal transport properties.

Contents

		Page
1.	**Introduction**	**1**
	Phenomenon of heat conduction	3
	Section A	**13**
	Theoretical background	13
1.1.	Basic definitions	13
1.2.	Material type and heat carriers	15
1.2.1.	Dielectric solids (insulators)	15
1.2.2.	Metals	19
1.2.3.	Superconductors	20
1.2.4.	Disordered materials	23
1.3.	Scattering mechanism	24
2.	**Theory of the method**	**28**
2.1.	Transient plane source method	28
2.1.1.	The basic equation of the hot disc sensor	28
2.2.	Deviation from the theory due to experimental factors	34
2.2.1.	Deviation due to design parameters of the sensor	34
2.2.2.	Negligible thickness and heat capacity of the TPS-element	35
2.2.3.	The influence of the insulating layer	35
2.2.4.	Neglecting the heat leak through the heavy electrodes	36
2.3.	Deviation due to the experimental setup	38
2.3.1.	Arrangement of the sample	38
2.3.2.	The basic circuit design	38
2.3.3.	The effect of other circuit components	40
2.3.4.	The leads resistance R_L	44
2.4.	Deviation from the theory due to improper data reduction	44
2.4.1.	Evaluation of the integral equation of the sensor	45
2.4.2.	Compensating for the time delay	45
2.4.3.	Compensating for the temperature drift	45
2.5.	Experimental setup and calibration measurements	48
2.5.1.	Experimental apparatus	48
2.5.2.	Low temperature measurements	50
2.5.3.	Temperature coefficient of resistivity of TPS-element	56
2.5.4.	Precautions	59

2.5.5. Calibration measurements 59
2.6. Preparation and characterizaion of high-T_C superconductors 65

3. Results and discussion 73

Conclusions 78

Appendices

Appendix 1 81
TCR (α) of the TPS-element
Appendix II 87
Values of the resistance for the Pt-resistance thermometer as a function of temperature (77-300K)
Appendix III 89
Thermal conductivity data of $YBa_2Cu_3O_{7-\delta}$
Appendix IV 90
Thermal conductivity data of fused quartz

References 91

CHAPTER 1

INTRODUCTION

The rapid advances in the field of thermal conductivity measurements of various materials during the last few years have stimulated the development of instrumentation. The instrument resolution has been improved by the construction of better heating element, power supplies, methods of computer enhancement of data calculation and with the use of vacuum system for low temperature thermal conductivity measurement apparatus comprising of better sample holder configuration.

Similar considerations govern the choice of materials preparation, particularly in more recent times under the impact of technology employing the results of scientific analysis of heat transfer. This reveals that the study of thermal conductivity often requires a context of materials science, in the widest sense. It will be clear that the existence of a body of data on thermal conductivity and related properties will never suffice to meet the problems posed by technology. What is also needed is theoretical understanding which will enable us to predict the thermal conductivity of new materials, and to guide us in our experimental attempts to find the materials to cope with new requirements. In turn the testing of a particular technique will challenge the experimenters by requiring new standards of accuracy and sophisticated apparatus for measurements.

The methods of measuring thermal conductivity can be divided in to two categories, static and dynamic, depending on whether the temperature distribution within the sample is time dependent. For static measurements it is necessary to determine the heat current density and the temperature gradient along the normal to the isothermal surface. In contrast to the steady state measurements, dynamic methods involve the complete differential heat flow. In general these methods determine the diffusivity and require measurement of the time for a thermal disturbance to propagate a known distance. The specific heat and density must be known in order to obtain the thermal conductivity, although in some dynamic methods the specific heat can be determined as well as the diffusivity. Both steady state and dynamic methods require the solution of the appropriate equation for the particular geometry of the sample, heat source, and sink. The simple solution involve isothermals which are either plane, cylindrical, or spherical surfaces. It is usually an experimental problem to maintain the isothermals of the shape required

for a particular mathematical solution, because of heat transfer from the sample to the surrounding medium.

The stationary state condition assists in the achievement of a high degree of precision of measurement, although the total time involved in achieving equilibrium can be a very lengthy process if the conductivity is low. The long time constant also makes steady state methods undesirable at very high temperatures. Dynamic methods, in general, don't give as high a precision as static ones although modern instrumentation is improving enormously the precision attainable with this type of method. There has been a tremendous upsurge of interest in various dynamic techniques in the past few years with the desire to obtain data rapidly, particularly at high temperatures.

The choice of method of measurement depend upon the order of magnitude of the thermal conductivity to be evaluated, on the temperature range, and on the sample size. As a result of the comparatively small range of thermal conductivities there is no thermal insulator in the sense of electrical insulator. Consequently, the problem common to all method of measurements is the attainment of the conditions of heat flow required by the mathematical solutions; moreover the degree of difficulty tends to increase with increasing temperature. As a note of caution it should be remembered that, if these conditions are not met experimentally, then the data acquired are meaningless.

However, this is an age of new materials and, since prediction of thermal conductivity is extremely difficult, it is a property which must be investigated experimentally. In order to make new data more reliable than those of the past, apparatus for the measurement of thermal conductivity or diffusivity should be thoroughly checked for systematic errors. Although these can be difficult to locate, they can sometimes be found by repeating measurements under different experimental conditions, changing for example the sample size or heat flux. The apparatus should finally be checked by measuring one or more materials of known thermal conductivity. There is no single reference material, but the standard or standards chosen to 'check' a particular apparatus should cover the full range of conductivities for which the apparatus is to be used. High-purity copper, Armco iron, various nickel alloys, particular glasses are commonly used. For work of

highest precision a bank of reference standards is being established at the National Bureau of Standards in Washington from whom details of stock material can be obtained. The report by Fitzer[1] serves as a useful guide to the choice of reference materials, some of which are readily available. For comparison with other materials, Fig.1.1 gives λ for some solids as a function of temperature, and Fig.1.2 gives the range of thermal conductivity of various substances at ambient temperatures and normal pressure[1].

When reporting thermal conductivity data as much information as possible should be given in order to characterize the material. This should include the source of the material, its chemical analysis, fabrication treatment, density, grain size, crystal structure, and direction of heat flow, together with details of shape, size, and orientation of any additional phases in heterogeneous materials.

One of the important properties of high-T_c superconductor materials is their ability to conduct heat. There is an obvious technological interest in how efficiently and by what means the heat flows in these solids. The magnitude and temperature dependence of the thermal conductivity are parameters which have an impact on a broad spectrum of devices[2].

From a theoretical point of view, the thermal properties of superconductors offers important clues about the nature of their charge carriers and phonons and scattering processes between them. In high-T_c superconductors such information is even more valuable due to the fact that traditionally galvanomagnetic probes such as resistivity, Hall effect and thermopower are inoperative in the wide temperature range upto T_c. The potential of normal state transport measurements to provide insight into the nature of superconductivity is thus drastically curtailed. No such limitation exists for the thermal conductivity and one has available the entire temperature range for gathering important transport data.

PHENOMENON OF HEAT CONDUCTION

The heat flux in solid consists in principle of two independent contribution: energy transport associated with the flow of charge carriers this is the electronic thermal conductivity, λ_e and the thermal energy carried by lattice vibration that is

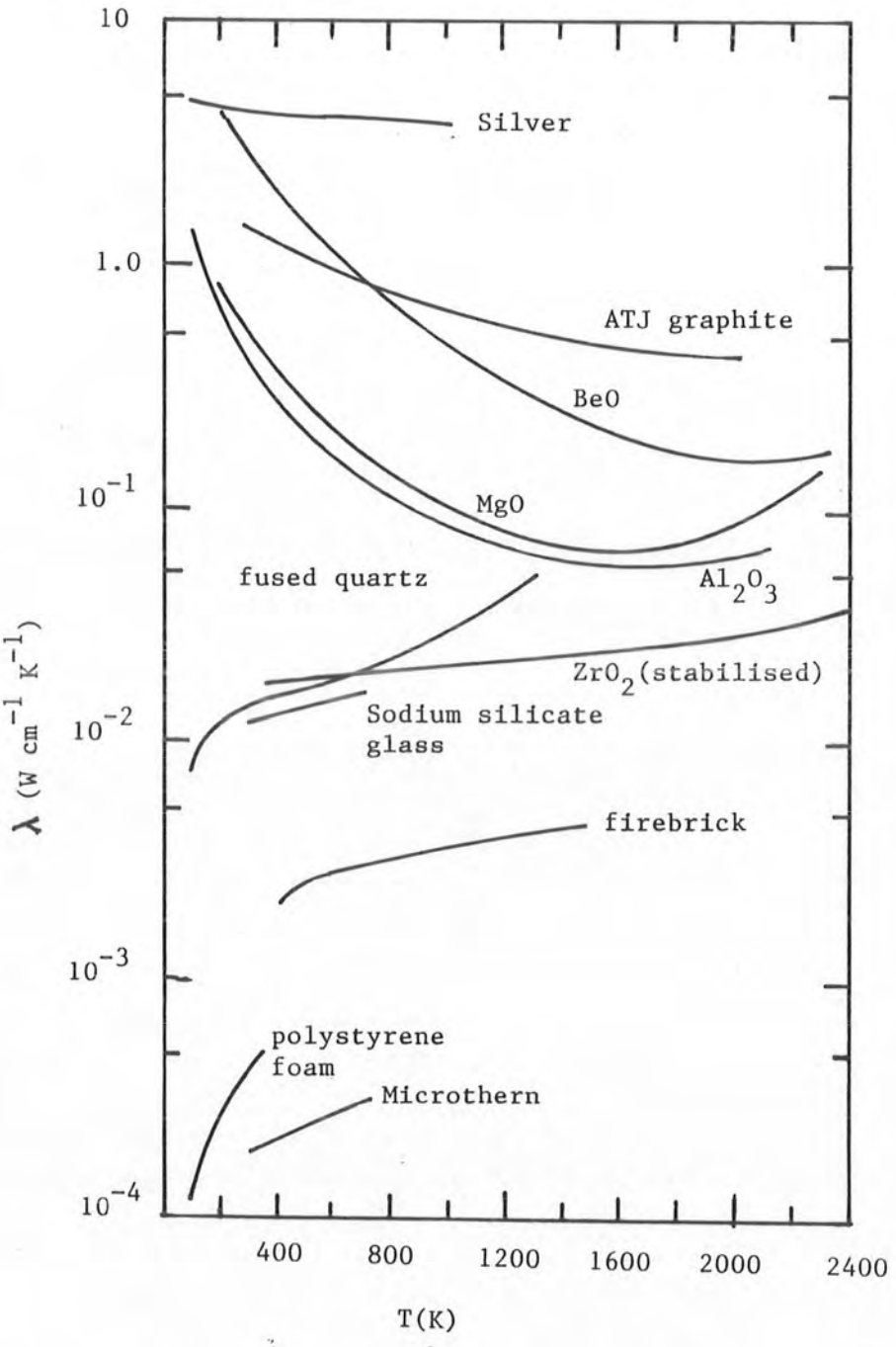

Figure 1.1. Thermal conductivity of various solids

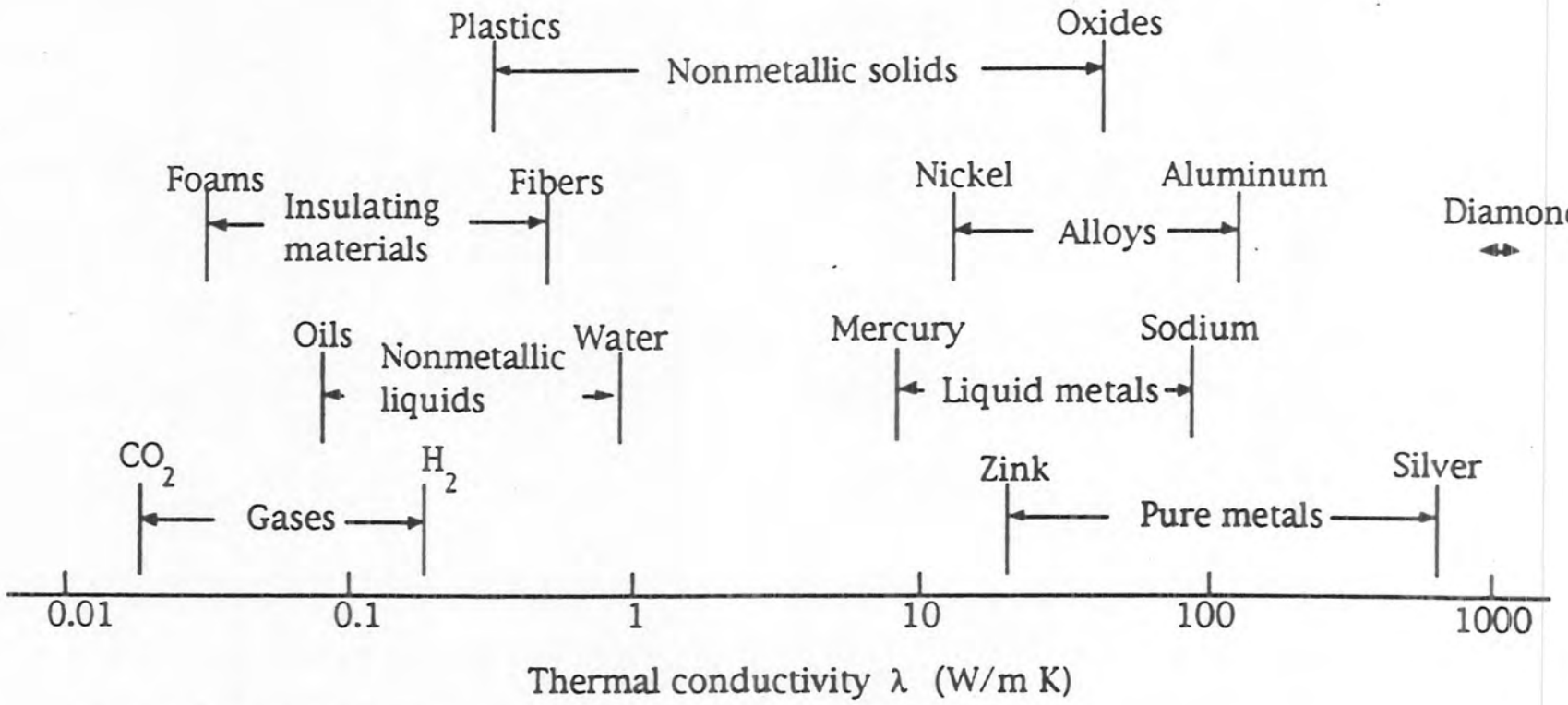

Figure 1.2 Range of thermal conductivity of various substances at ambient temperatures and normal pressure.

known as the lattice or phonon thermal conductivity λ_p. The total thermal conductivity is then

$$\lambda = \lambda_e + \lambda_p \tag{1.1}$$

The relative magnitude of the two contributions in Eq. (1.1) can be used to classify various types of solids in a way analogous to the magnitude of the electrical resistivity. Thus in insulators, there are no free charge carriers (λ_e=0), and consequently, $\lambda = \lambda_p$. While lattice vibrations also contribute to the thermal conductivity of the metals, strong scattering of phonon on free carriers drastically suppresses the lattice contributions in this case and the total thermal conductivity is essentially entirely due to charge carriers. The purer the metal, the smaller the relative contribution of phonons[9].

A remarkable feature of superconductors is the fact that, while in their normal state ($T > T_c$), the carrier contribution typically greatly exceeds the lattice term λ_p, at low temperature well below T_c, their thermal transport resembles that of a dielectric solid. It is in the intermediate temperature range, from $0.3T_c \approx T_c$, that the consideration of electrons into a Cooper pair sea plays a decisive role in the interplay between the electron and phonon heat conducting channels. This is temperature region on which most of the experimental work has centered and turn out to be the domain where high-T_c superconductors show a spectacular variation in their thermal conductivity. It is worth noting that flux quantization measurements on high-T_c superconductors indicate a charge 2e.

It is important to realize that even if one of the two conducting channels, that is λ_e or λ_p does not dominate the heat transport, the phonons do effect the magnitude and temperature dependence of the electrical contribution. Likewise, the presence of free carriers, even of relatively low density so that λ_e is small, strongly modifies the flow of phonons. The phonons for this behavior are relaxation mechanisms that ensure the satisfactory nature of the heat conducting process. For instance, the charge carriers are scattered by phonons, yielding the electronic thermal resistivity $W_{e,p}$, by static imperfections such as impurities, stacking faults,

grain boundaries, voids, etc., that lead to a term $W_{e,d}$ and by other electrons, $W_{e,e}$. According to the Mattheissen's rule, the scattering processes for each homogeneous group of electrons are additive, so that the electronic thermal conductivity is given by

$$\frac{1}{\lambda_e} \equiv W_e = W_{e,p} + W_{e,d} + W_{e,e} \tag{1.2}$$

Similarly, phonons of a given sample are scattered by different mechanisms, some of which are listed below with their associated scattering rates:

(i) Scattering at the specimen boundaries, $\tau_{p,b}^{-1}$

(ii) Scattering by two-level tunneling states, $\tau_{p,t}^{-1}$

(iii) Scattering by dislocations $\tau_{p,r}^{-1}$

(iv) Scattering by point defects, $\tau_{p,d}^{-1}$

(v) Scattering by free electrons, $\tau_{p,e}^{-1}$

(vi) Scattering by other phonons, $\tau_{p,p}^{-1}$

As in the electronic case, the total scattering rate τ_p^{-1} for the phonon is found by summing over all the phonon scattering processes listed above. It is often necessary to consider the frequency (ω) and polarization (i) dependence of the phonon scattering rate $\tau_p^{-1}(\omega)$, in which case one usually regards phonons of different frequency as different heat conducting channels and sum their contributions to get the total phonon thermal conductivity. Using the elementary kinetic formulation, we obtain [1]

$$\lambda_p = \frac{1}{3}\sum_i \int_0^\infty C_i(\omega)\ v_i^2(\omega)\ \tau_{p\,i}(\omega)\ d\omega \tag{1.3}$$

where $C_i(\omega)$ is the lattice heat capacity per unit volume for phonons of angular frequency ω and $v_i(\omega)$ is the speed of the ith mode. Within the Debye framework of lattice dynamics, neglecting polarization dependence, Eq.(1.3) becomes

$$\lambda_p = \left[\frac{k_B^4}{2\,\nu\pi^2\hbar^3}\right] T^3 \int_0^{\Theta_D/T} \tau(x) \left[\frac{x^4 e^x}{(e^x-1)^2}\right] dx \qquad (1.4)$$

where $X = \frac{\hbar\omega}{k_B T}$ is the phonon energy, Θ_D is the Debye temperature, and ν (constant) is the speed of sound. For each scattering process of electrons and of phonons, one can calculate both its magnitude and temperature dependence and in principle, solve the thermal conductivity problem. In practical situations not all scattering processes act at the same time. One then attempts to select one or two major dissipative mechanisms and determine their scattering strength empirically by fitting to the experimental data. For instance, a normal metal can be modeled by the expression

$$\frac{1}{\lambda_e} \equiv W_e = aT^2 + \frac{b}{T} \qquad (1.5)$$

where the first term on the right-hand side of Eq. (1.5) stands for the electron scattering by phonons and the second term represents the interaction of electrons with static defects in the metal lattice. By plotting $\frac{T}{\lambda_e}$ versus T^3 one can readily determine the coefficients a and b. The functional form of Eq. (1.5) is, indeed, a rather good representation of thermal conductivity of pure metals. The lattice thermal conductivity of the metals and alloys is determined primarily by the combined effect of the phonon-phonon U-processes that lead to a T-linear lattice resistivity contribution near and above the Debye temperature Θ_D, and the phonon-electron interaction that at low temperature is well approximated by a T^{-2} resistivity term. It then follows that at sufficiently high and also at rather low temperatures the lattice thermal conductivity of metals and alloys is quite small. It is in the intermediate temperature range where the phonon contribution may rival the electronic thermal conductivity.

There are two fundamental properties of superconducting condensate that have an overriding effect on the thermal conductivity of a superconductor:

1. Cooper pairs carry no entropy.
2. Cooper pairs do not scatter phonons.

The first condition means that the electronic thermal conductivity vanishes rapidly below T_c. This is immediately obvious if one invokes a kinetic theory formulation of the electronic thermal conductivity

$$\lambda_e = \frac{1}{3} C_e V_e \ell_e \tag{1.6}$$

where C_e is the specific heat of the carriers, V_e their Fermi velocity, and ℓ_e their mean-free path. While V_e is essentially constant and ℓ_e varies as a power law of temperature, the dominant contribution comes from the specific heat that at $T < T_c$ decreases approximately exponentially.

The second condition has a more subtle effect on the thermal conductivity of superconductors. Provided that the mean-free path of phonons at $T > T_c$ is limited by scattering on charge carriers, on passing into the superconducting state the thermal conductivity will rise because the number of quasi-particle excitations rapidly decreases leading to an enhancement in the mean free path of phonons, ℓ_p. A competition between the rapidly diminishing λ_e on the one hand and increasing λ_p on the other will determine the overall dependence of the total thermal conductivity of a given superconductor. In the vast majority of the cases (all pure conventional superconductors and most alloys) λ falls rapidly as the material goes superconducting. This general trend encompasses both weakly and strongly coupled superconductors. In the latter case, the decrease in the thermal conductivity is more rapid as a result of a larger prefactor γ in the temperature dependence of the energy gap Δ,

$$\left(\frac{\Delta}{k_B T}\right)_{T \to T_c} = \gamma \left(1 - \frac{T}{T_C}\right) \tag{1.7}$$

According to the BCS theory [4], $\gamma = 3.06$, while for a strong coupling material like lead the prefactor is $\gamma \approx 4$. in some alloys, sufficiently disordered so that λ_e is small and λ_P accounts for a large fraction of the normal-state thermal conductivity, one may observe a rise in the total conductivity as the sample enters into its superconducting domain. A classic example of this trend is lead-10% bismuth alloy [3]. Eventually, of course, the thermal conductivity must turn over and start decreasing as a function of temperature. This follows because the phonon population decreases as T falls, and phonon-defect scattering starts to dominate the transport at low temperatures.

As the phase transition at $T = T_c$ affects both the electronic and lattice thermal conductivities. since the phonon contribution in high-T_c superconductors overwhelmingly dominates the total thermal conductivity even in the normal state, it is the decrease in phonon-electron scattering rate which is responsible for the change in the thermal conductivity as the sample is cooled past its transition temperature. The theoretical description of the behavior of the lattice thermal conductivity limited by carrier scattering was developed originally for the BCS model by Bardeen, Rickayzen and Tewordt, the so called BRT theory in [4]. Tewordt and Wolkhausen [5] have recently supplemented this theory by taking into account additional phonon scattering processes that might be appropriate when describing phonon transport in high-T_c superconductors. Tewordt and Wolkhausen have used this model to the strength of the phonon-electron interaction. In principle, this theory should be very valuable for estimating anisotropy in phonon-electron coupling once reliable data on the thermal conductivity of single crystals in the c-direction become available.

The development of theory and construction of the thermal conductivity measuring apparatus has influenced the lay out of this dissertation. The major work in this thesis is devoted to construction and calibration of low temperature thermal conductivity measurement apparatus and then applying Transient Plane Source (TPS) technique to measure thermal properties of solids at low temperature, also to probe new physical phenomenon such as the enhancement of thermal conductivity of high-T_c superconductors at the transition temperature.

The TPS technique offers the possibility to measure thermal properties which are directly related to heat conduction such as thermal conductivity λ, thermal diffusivity κ and specific heat C. The knowledge of such properties requires techniques that can perform such investigations and suit their major aspects. This can be achieved either by introducing new techniques or extending and modifying the existing ones, so that they become more reliable and easy to operate.

The first chapter is an introduction to the main contents of the dissertation with a brief discussion of the basic principles of the static and dynamic methods of measuring thermal conductivity, with emphasis on the measuring accuracy of an apparatus from calibration point of view and section A is an overview of the theoretical background relevant to the discussed topics in the dissertation with some preliminary questions of definition and so forth.

Chapter two covers a detailed discussion of the construction of the thermal conductivity measurement apparatus following the TPS technique with a special reference to instrumentation involved in the method theory. The theory of the TPS method is described and is elaborated upon the principle of thermal conductivity of solids. The experimental design criteria along with the experimental setup and procedures needed to account for the deviations of the experiment from theory is briefly described. A small portion is devoted to the preparation of high-T_c superconductor $YBa_2Cu_3O_{7-\delta}$ sample in bulk polycrystalline form and the characterization of this ceramic oxide superconductor by Meissner effect, electrical resistivity, etc.. It includes the calibration process performed with fused quartz sample in the temperature range 77-280K. These measurements show that the TPS technique can be used successfully down to liquid nitrogen temperature.

Chapter 3 includes the measurements performed on steel sample at room temperature. Results and discussions on the thermal transport properties and electrical resistivity of superconducting sample $YBa_2Cu_3O_{7-\delta}$ has been described with respect to electron-phonon interaction around T_c, a possible mechanism involved in the heat conduction of high-T_c superconductors. Lastly, it contains deduced conclusions of the dissertation which consist of the essence of

understanding and development obtained from the present research work together with the suggestions for further investigations.

SECTION A

THEORETICAL BACKGROUND

1.1 BASIC DEFINITIONS.

In 1822 Fourier was the first to give a clear statement about the proportionality of heat flow (Q) and temperature gradient. The general form of Fourier's law describing the heat current density (J) in solids at steady state condition is [1,6,7,8]

$$J_i = -\sum_j \lambda_{ij} \frac{\partial T}{\partial x_j} \tag{1.8}$$

where λ_{ij} is the thermal conductivity (the ability of the material to transport heat in all directions), a tensor of second rank having nine components and assumed to be temperature independent, and $\frac{\partial T}{\partial x_j}$ is the temperature gradient in the jth direction. If we neglect the anisotropy with respect to the heat conduction, as in case of polycrystalline and cubic crystals, the above equation can be rewritten as

$$\mathbf{J} = -\lambda \ \mathbf{grad}\ T \tag{1.9}$$

The negative sign indicates that heat flows down, a temperature gradient from the hotter to the colder regions.

It should be noted that the above equations are defined with respect to regions where the fluctuations in J and grad T are negligibly small. These vectors , **J** (measures the rate of flow of heat across unit cross-section perpendicular to **J**) and **grad T**, should be considered at a "microscopic" level in the solid. Furthermore, open circuit conditions are assumed during the heat conduction, i.e. we are neglecting the thermoelectric effects. The S.I. units of thermal conductivity

are $Wm^{-1}K^{-1}$ and the values expressed in these units are 100 times greater than those given with the centimeter as unit of length $Wcm^{-1}K^{-1}$.

To define thermal diffusivity, which is another frequently used thermal transport parameter, we need to apply the principle of conservation of energy. If we consider an infinitely small volume element inside the conducting medium, the change in its internal energy ΔU at time t will be given by the heat transfer across the surface boundaries of this element and can be expressed as

$$\frac{d(\Delta U)}{dt} = -\int J \cdot n \; ds \tag{1.10}$$

where n is the outward normal of the surface. Now using Gauss's Law, and replacing the left hand side by the volume integral over the internal energy density U, we get

$$\int \frac{\partial U}{\partial t} d^3x = -\int divJ \; d^3x \tag{1.11}$$

Since the volume integration is arbitrary then

$$\frac{\partial U}{\partial t} = -divJ \tag{1.12}$$

The changes in internal energy can be expressed in terms of the specific heat per unit mass C multiplied by the density ρ.

$$\frac{\partial U}{\partial t} = C\rho \frac{\partial T}{\partial t} = -divJ \tag{1.13}$$

where C is defined as the amount of heat flow into the system per unit mass (or mole) per the corresponding change in temperature. Combining Eq. (1.13) with Eq. (1.9), We get

$$\frac{\partial T}{\partial t} = \kappa \nabla^2 T \tag{1.14}$$

Where ∇^2 is the Laplacian operator and $\kappa = \lambda/\rho C$ is thermal diffusivity ($m^2 s^{-1}$) which can be seen as a measure of the response of the medium to a thermal

perturbation. This is the basic equation of heat conduction for non-steady state or transient type measurements.

1.2 MATERIAL TYPE AND HEAT CARRIERS

In principle the different materials may be classified according to their ability to conduct heat similar to their ability to conduct electricity. However, the analogy is not perfect. For instance, diamond which is known to be an electrical insulator is one of the best known heat conductors at room temperature, see Fig. 1.2.

The general reason for this diversity is related to the fact that electricity is carried by electrons, while heat is mainly carried by electrons in metals, by phonons in insulators, by magnons in magnetic materials, and by photons in radiative processes. In fact, some or all of the above carriers could be combined in one type of material. This gives an indication of the complication to deal with heat transport mechanisms, especially when we have to include the interaction (scattering) between these carriers, and the effect of structure of the material on each type of carrier, all of which might be temperature dependent. In this work we will only focus on phonons and electrons with emphasis on their interactions and scattering mechanisms.

1.2.1 DIELECTRIC SOLIDS (INSULATORS)

The simplest way to understand the transport of heat in dielectric materials is to choose a perfect electrical insulator and look at the internal energy of this material, which is manifested in the thermal motion of atoms, or commonly referred to as lattice vibrations. By using a model for the solid. Where the atoms are coupled to their neighbors by forces, the thermal vibrations may be considered as normal modes obeying harmonic oscillator equations. These harmonic oscillators are found to possess energy only in integer units of $h\upsilon = \hbar\omega$, where υ is the oscillator frequency and $\hbar$ is Planck's constant. These quanta $\hbar\omega$ are called phonons in the solid by analogy with photons of electromagnetic radiation. Thus, there are two pictures to describe the heat conduction in solids, namely either as

varying amplitudes of the lattice vibrations (waves) in hotter and colder regions, or as transport of phonons (particles) from a hotter region (where they are abundant) to a colder region (where they are less numerous).

In a solid with crystalline symmetry the normal modes can be described as traveling waves characterized by a particular frequency ω and by two additional vectors: the wave vector q which defines the direction of propagation with a magnitude equal to the reciprocal of the wavelength times 2π, and the polarization vector s which refers to the direction of the atomic displacements. The frequency ω can be written as a function of q and s i.e.,

$$\omega = \omega_s(q)$$

The properties of phonons as particles can be summarized as:

(I) Like a conventional particle they have momentum and energy .

(ii) They have no mass, and they are not conserved in the same way as atoms or electrons are.

(iii) The total number of phonons is not fixed, although their total energy is.

(iv) All phonons of the same mode are indistinguishable i.e., they obey Bose-Einstein statistics.

Lattice vibrations at low frequency (long wavelength), can be identified with sound waves in crystal, and if v_s is the velocity of sound for a wave of polarization s, then

$$\omega = v_s q \qquad (1.15)$$

As the wavelength decreases this relation breaks down and ω usually falls below $v_s q$. This relation between ω and q is called the dispersion relation [1,6,7,8]. It can be determined experimentally and is illustrated in Fig.1.3 for a one dimensional lattice with two atoms per unit cell. For a unit cell with dimension a, the only allowed values of q are within the range $-\pi/a < q > \pi/a$. The modes of vibration illustrated by the lower curves, which vanishes as $q \rightarrow 0$, are called acoustic modes because of their connection with propagation of sound, while the other modes given by the upper curves are called optical modes because their

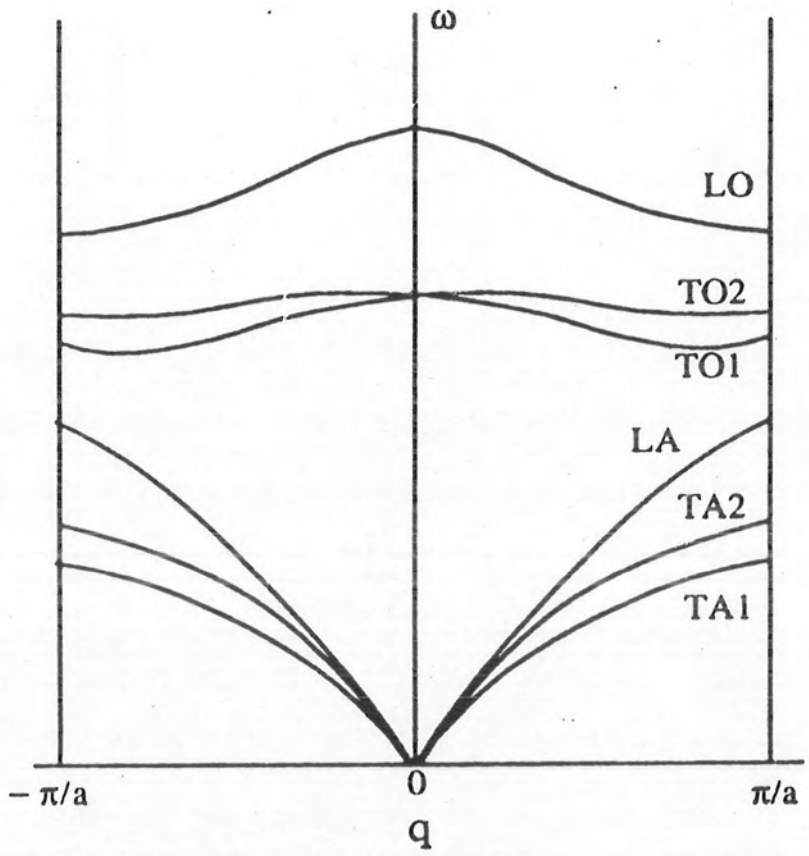

Fig. 1.3 The phonon dispersion curves for two atoms per unit cell.

frequencies are in the infrared range. Within each range of both optical and acoustic modes there are one longitudinal and two transverse (modes) vibrations. The atomic displacement is parallel to q in the former, and it is normal to q and to each other in the later.

At this point it is worth to mention that in dielectric solids, depending on their temperatures, the heat conduction can be described by different regimes. At low temperature where collective vibrations (long wavelength vibrations or small q) predominate, and the propagation resembles the elastic (sound) waves, the regime is called collective, while at high temperature where individual vibrations are abundant, the energy of the individual vibration is carried by a random walk through the solid and the process can be described by the diffusion equation, the regime is called diffusive.

One of major tasks in the theory of solids is to determine the dispersion relation $\omega_s(q)$. According to Debye's model, which implies that the dispersion relation should follow Eq.(1.15), the constant frequency surfaces in (three dimensional) q-space will become spheres. Within this limit (Debye's limit), the number of available modes in a crystal of volume V, or formally called the density of states $g(\omega)$, is given by:

$$g(\omega) = \begin{cases} 0 & \omega > \omega_D \\ \dfrac{3V\omega^2}{2\pi^2 v^2} & \omega < \omega_D \end{cases} \qquad (1.16)$$

Knowing the density of states and the distribution function $n(\omega)$ (Planck's distribution) for phonons, the internal energy could be calculated by integrating over the Debye's frequency (ω_D) range.

$$U = \int d\omega g(\omega) n(\omega)\ \hbar\omega = \frac{3V\hbar}{2\pi^2 v^3} \int_0^{\omega_D} \omega^3 \left[Exp\left(\frac{\hbar\omega}{k_B T}\right) - 1 \right]^{-1} d\omega \qquad (1.17)$$

By means of U the other properties can be determined, for instance the specific heat C(ω) is directly deduced from $\frac{\partial U}{\partial T}$, and then the lattice thermal conductivity (λ_L) can be expressed as[6,9]

$$\lambda_L(T) = \frac{1}{3} v^2 \int_0^{\omega_D} \tau(\omega)\ C(\omega) d\omega \qquad (1.18)$$

where $\tau(\omega)$ is the relaxation time of all the phonon scattering processes.

1.2.2 METALS

The simplest way to understand the transport of heat in metals is to choose a pure metallic sample where electrons are playing the major role in electrical and heat conduction processes. In fact it was suggested by Wiedemann and Franz that for metals, at not too low temperatures, the ratio of the electronic thermal conductivity (λ_e) to the electrical conductivity (σ) is directly proportional to the temperature, with the constant of proportionality (Lorenz number) being independent of the particular metal [8], i.e.,

$$\frac{\lambda_e}{\sigma T} = \frac{\pi^2}{3}\left(\frac{k_B}{e}\right)^2 = 2.45 \times 10^{-8}\ \text{watt} - \text{ohm}/\text{deg}^2 \qquad (1.19)$$

The Wiedemann Franz law is based on the assumption that under the influence of an electric field, the average distance traveled by free electrons without collisions (the electron mean free path ℓ_e) is the same as the corresponding average distance traveled under the influence of a temperature gradient. However, in order to understand the role of electrons in these conduction processes, a quantum mechanical treatment is needed to reveal the details of such processes.

According to quantum mechanics there are certain states available for electrons to occupy which are specified by a wave vector k and energy ε. The allowed values of k are similar to those of q in the lattice vibration case. Since each value of k has many values of ε and the energy levels are grouped into bands

with gaps (no permitted energy states) between these bands. We can express the energy in terms of the wave vector k and the band index b as $\varepsilon_b(k)$. A simplified form of energy bands is shown in Fig.1.4

At this point it is worth mentioning some of the important properties of electrons as distinct particles:

(i) According to the Pauli's Exclusion Principle each energy level can accommodate two electrons owing to their two allowed spin orientations.

(ii) The number of electrons is constant since it is determined by the condition of electrical neutrality of the atoms in the solid.

(iii) Energy will be available for them at all temperatures above absolute zero and the probability of finding an electron at energy ε is following the Fermi distribution function $f_0(\varepsilon)$. Nevertheless, at absolute zero there will be an energy $\left(\varepsilon_F\right)$ below which all the states are filled.

Using the density of states $N(\varepsilon)$ for electrons, we can calculate the total energy E of electrons in a similar fashion as we did in the case of phonons

$$E = \int d\varepsilon \; N(\varepsilon) \; f_0(\varepsilon) \; \varepsilon \qquad (1.20)$$

Here, the electronic specific heat is given by $\frac{\partial E}{\partial T}$.

1.2.3 SUPERCONDUCTORS

One class of materials where both electrons and phonons play a role in heat conduction is superconductors. Therefore we will discuss the electronic and the lattice thermal conductivities and their relationship to one another in this class of materials [6,7,10]. Since electrons and phonons take part directly in the transport of energy, we may write the total thermal conductivity λ to be equal to the sum of two components one of which is due to lattice conduction and the other is due to conduction by charge carriers.

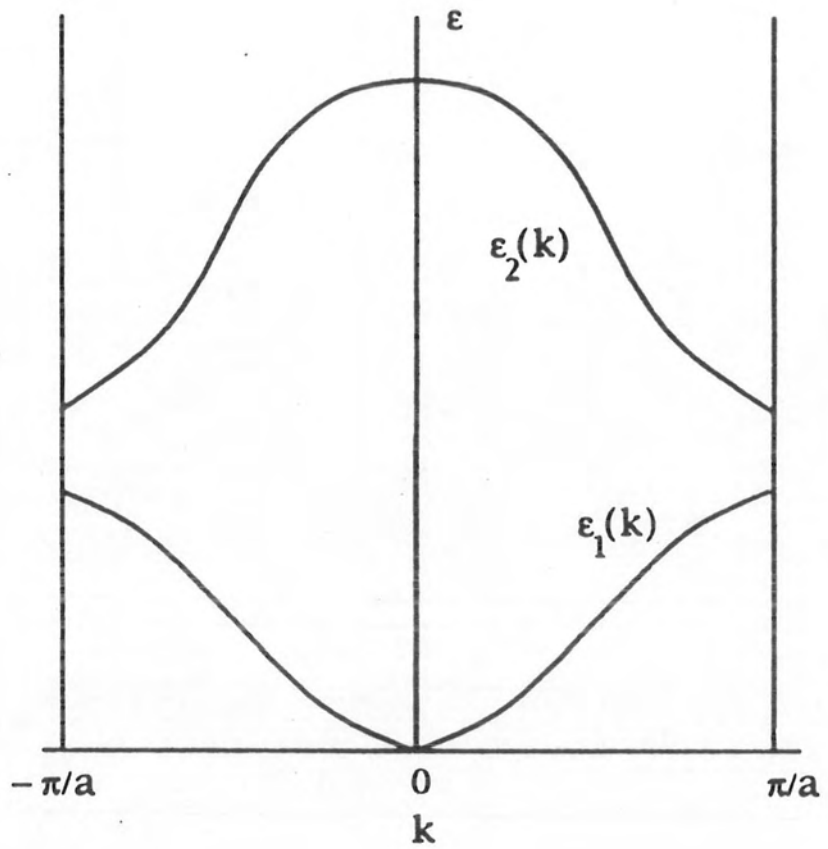

Figure 1.4 Simplified band structure in solids.

$$\lambda = \lambda_c + \lambda_L \tag{1.21}$$

In superconductors in general (including the conventional low-T_c superconductors), the thermal and kinetic properties in the superconducting state[11], differ from those properties in the normal state. The basic difference follows from the way the electrons behave below T_c. In particular the electrons which take part in the condensation process, "superconducting electrons", become unable to transport thermal energy and to interact with phonons. The other electrons, which do not take part in the condensation process (normal electrons), will preserve their properties as in the normal state, and they can transport and absorb thermal energy, and in addition they will be scattered due to interaction with phonons.

Thus, the kinetic phenomena in superconductors have a particular character, related to the dependence of the number of the electron excitations on temperature. Moreover, the strength of interactions between elementary excitations, or the appearance of singularities connected with phase transitions, and other prerequisites presently not known, can also alter the kinetic phenomena by causing anomalies in the thermal and other physical properties in these materials.

In conventional low-T_c superconductors the major role in the thermal conduction may be played by the electron component [6,7] of the thermal conductivity when T approaches T_c. On the other hand, according to Eq.(1.19) turned out to be rather inconsiderable in high-T_c. superconductors (10-15%) [12,20,21], compared to the total thermal conductivity, and the decisive contribution the thermal conductivity may come from the phonon (lattice) part both above and below T_c. Further interesting details are the presence of particular characteristics such as the sudden change of the slope of $\lambda(T)$ at the phase transition, the appearance of the temperature dependence of the thermal conductivity on the oxygen content [12], and the linear response of the electrical resistivity above T_c [12,20,21], all of which are part of the distinct features of high-T_c superconductors.

Utilizing the measured data of thermal and electrical conductivities of high-T_c superconductors both in the normal and superconducting states makes it

possible to estimate the value of the coupling constant which is a parameter related to the strength of the phonon-electron interaction [12]. According to the conventional BCS theory, the phonon-electron interaction below T_c is effectively an attractive interaction between electron pairs of opposite spin and wave vector via an exchange of phonons. This attractive interaction will result in the formation of Cooper pairs and a superconducting gap.

The magnitude of this coupling constant (strength of the interaction) may indicate that physical mechanism causing the sudden change in the slope of $\lambda(T)$ are in agreement with the prediction of the generalized Bardeen-Rickayzen-Tewordt (BRT) theory [13,14].

1.2.4 DISORDERED MATERIALS

This is rather large class of materials including all amorphous solids such as glasses, and it is characterized by short-range order in its internal structure. In these materials the phonon mean free path for short wavelengths may be limited by the dimensions of the structure units such as grains, or by the size of the extended defects such as dislocations or stacking faults. Although the major contribution of thermal conduction of these solids is attributed to the lattice conduction, the choice of an appropriate theoretical model to predict the thermal conductivity requires a detail knowledge of its microstructure, and most often the thermal conductivity can only be obtained experimentally.

A special class of materials is polycrystalline ferroelectrics of the potassium dihydrogen phosphate (KDP) family type. This type of material also shows a phase transition of para-ferro type. The changes taking place during the transition from the paraelectric to the ferroelectric state are due to the influences from the phase transition[12] mechanisms (displacement and order disorder) on mean free path of the phonon during the conduction process. The thermal conductivity measurements revealed that these mechanisms are predominant over the other scattering mechanisms, which are due to intrinsic microstructure disorder such as grain boundaries and porosity (voids).

1.3 SCATTERING MECHANISMS

The general character of the temperature dependence of the thermal conductivity is connected with the temperature dependence of the mean free path of the heat carriers. It depends upon the different type of the scattering mechanisms involved in the heat conduction processes. Moreover these mechanisms are contributing to the magnitude of the thermal resistance. In order to estimate this resistance using certain theoretical models[6], it may be necessary to define relaxation times of these mechanisms.

Assuming that the transport of thermal energy is carried mainly by phonons and electrons, we can according to Eq.(1.21) express the total thermal conductivity λ as

$$\lambda = \lambda_e + \lambda_p = \left[\frac{1}{\lambda_e^d} + \frac{1}{\lambda_e^p} + \frac{1}{\lambda_e^e}\right]^{-1} + \left[\frac{1}{\lambda_p^d} + \frac{1}{\lambda_p^e} + \frac{1}{\lambda_p^p}\right]^{-1} \qquad (1.22)$$

where the superscripts e, p and d refer to electrons phonons and defects respectively. The first three mechanisms are referred to an electron scattering on defects λ_e^d, on phonons λ_e^p and on electrons λ_e^e and the last three are phonon interaction with defects λ_p^d, with electron λ_p^e and with phonons λ_p^p respectively. In general, each of the mechanism is characterized by its temperature dependence which makes it difficult to interpret the experimental data. However, in most cases, within the attainable experimental condition, the state of substance, its structure and its temperature are fairly well known which make it possible to anticipate the dominating mechanism(s) with respect to other scattering process(es).

In the sample which we have studied the major role in heat conduction has been due to lattice thermal conductivity. Thus the focus will be on phonon scattering mechanisms. The defect term λ_p^d in Eq.(1.22) is related to various types of defects, such as point defects (vacancy ,interstitial or substituting atom....), dislocations (edge, screw, mobile, strain fields....), large defects(voids , inclusions, clusters..). The knowledge of how various types of defects scatter phonons is essential if one wants an accurate expression for the resulting conductivity.

However, the actual size of the defect is decided by the phonon wavelength which is of the order of Θ_D / T interatomic distances, where T and Θ_D are the specimen and Debye temperatures respectively [6]. In other words if the defect is large than a few inter atomic spacing, then the low frequency (long wavelength) will see it as a point defect. In cases where Rayleigh (point defect scattering is the dominant one, the total relaxation time of point defects may be limited to the relaxation time of point defects alone, which is proportional to $\omega^4 T^4$[6].

The phonon-phonon interaction term λ_P^P may be estimated by assuming a single-mode relaxation time, from which scattering mechanisms involving three phonons may be defined. They are of two kinds: either that two phonons (q_1,s_1) and (q_2,s_2) combine to give a third phonon (q_3,s_3) or that one phonon (q_1,s_1) breaks up to give two phonons (q_2,s_2) and (q_3,s_3). These processes can be perceived most clearly in their simple form by referring to the wave picture at long wavelengths, where the enharmonic (non-linear or cubic) terms in the lattice potential are related to the strain dependence of the elastic constants. and therefore to the velocity of sound. Thus a sound wave will produce a periodic variation in the sound velocity in a medium, and this will perturb the passage of a sound wave. Similarly, the second wave will perturb the first one, giving a symmetrical interaction. These non-linear interactions occur over the whole volume of the medium, which requires the involvement of different wave vectors. The best analogy to this perturbation is that the first sound wave acts as a diffraction grating for the second, so that there will be interference conditions involving q_1, q_2 and q_3.

The energy and momentum conservation in these two kinds of three phonon processes (using the relations $E = \hbar\omega$ and $P = \hbar q$) are

$$\omega_1 + \omega_2 = \omega_3 \text{ and } q_{1+}q_2 = q_3$$

$$\omega_1 = \omega_2 + \omega_3 \text{ and } q_1 = q_2 + q_3 + G$$

According to the wave picture, the lattice acts as a diffraction grating in the same manner as in X-ray crystallography. Therefore, to satisfy the total interference

condition and to account for the atomic nature of the medium (existence of the lattice), the lattice translation vector G has been added to the second momentum equation.

For cases when G = 0 the process is called normal or N process, and for cases when G ≠0 it is called Umklapp or U-process. Umklapp processes must be regarded as a combination of three-phonon processes and Bragg reflection. It should be noted that the N-processes (conserve) do not reduce the momentum or heat flow of the phonon gas, and in principle, these processes alone cannot produce non-vanishing thermal resistance.

The detailed theory, involving the role of the three-phonon N-processed is quite complicated, and will not be discussed here. However, these processes frequently enhance the effect of the remaining scattering mechanisms (do not conserve momentum), or they can shift energy and momentum from one group of lattice waves to another, for example from phonons which are weakly scattered to others which are strongly scattered, thus contributing indirectly to the thermal resistance. According to analysis done by Callaway [1,12] of the experimental conductivity data for imperfect crystals, the relaxation times of the N-processes and U-processes can be proportional to ωT^4 and $\omega^2 T^4$ respectively.

The phonon-electron interaction term λ_p^e is vital in the cases where the phonon and electron thermal conduction processes are competing, particularly when the conduction of phonons is limited by electrons as it might be the case of high-T_c superconductors. The effective role of this term is highly dependent on the nature of the interaction (weak or strong) and according to the BRT theory [13,14,16,17] it is proportional to $xTg(x,T)$ where $x = \hbar\omega / k_B T$ is the reduced phonon energy. The function $g(x,T)$ itself is proportional to the ratio of the phonon-electron scattering times in the normal and super conducting states $\frac{\tau_{pe}^n}{\tau_{pe}^s}$ being equal to unity in the normal state, and it is a universal function of $\Delta / (k_B T)$ in the super conducting state, where Δ is the super conducting gap.

Finally, the combined effect of all the above-mentioned scattering mechanisms can be expressed in terms of a total relaxation time, which is the reciprocal addition of the individual relaxation time of each mechanism.

$$\tau^{-1}(T,x) = S_b + S_d(x,T)^4 + S_e x T g(x,T) + S_p x^2 T^4 \qquad (1.23)$$

where the coefficients S_b,S_d,S_e and S_p describe the magnitude of the phonon scattering by boundaries, point defects, carriers and other phonons, respectively. This expression may be combined with the relevant equations in section 1.2.1, in order to estimate the lattice thermal conductivity.

CHAPTER 2

THEORY OF THE METHOD

EXPERIMENTAL SETUP

AND

CALIBRATION MEASUREMENTS

THEORY OF THE METHOD

2.1 TRANSIENT PLANE SOURCE METHOD

The theory of the method is based on a three dimensional heat flow inside the sample, which can be regarded as an infinite medium, if the time of the transient recording is ended before the thermal wave reaches the boundaries of the sample. The experiment is performed by recording the voltage variations over the TPS-element while its temperature is slightly raised by a constant electrical current pulse. Similar to the THS method, the time dependent resistance of the TPS-element during the transient recording can be expressed as

$$R(t) = R_0 [1 + \alpha \Delta T(t)] \qquad (2.1)$$

where R_0 ($\approx$ 3.67 Ω at room temperature) is the resistance of the TPS-element before the transient recording has been initiated. α is the temperature coefficient of resistance (TCR) for TPS-element (TCR $\approx$ 5.0 $\times$ 10^{-3} K) at room temperature and $\Delta T(t)$ is the time dependent temperature increase of the TPS-element. A typical temperature (voltage/resistance) recording versus time is shown in Fig. 2.1

Depending on the temperature range of interest, the TCR values for the TPS-element are determined within that particular temperature range from separate calibration procedures by means of a Pt-thermometer (See Appendix 1).

The assessment of $\Delta T(t)$ in the heater depends on the power output in the TPS-element, the design parameters of the sensor and the thermal transport properties of the surrounding sample. For the disk-shaped sensor $\Delta T(t)$ is given by the following equation derived as under, from which the thermal conductivity and diffusivity can be obtained.

2.1.1 THE BASIC EQUATION OF THE HOT DISK SENSOR

Both the thermal conductivity and diffusivity of the medium surrounding the TPS-element can be determined from the single transient event by recording the

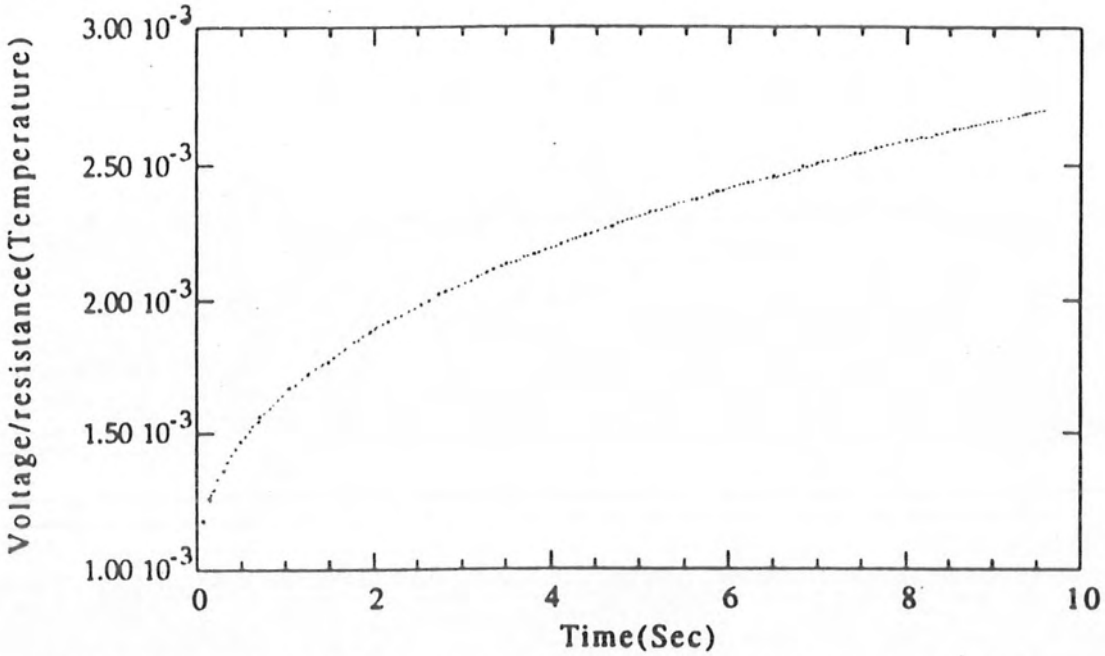

Figure 2.1 A typical temperature (voltage/resistance) recording versus time.

transient voltage while passing the current pulse through the element. In order to show this, we need to go on details in deriving the basic equation of the TPS method using the hot-disk configuration.

The differential equation of conduction of heat in three dimensions is

$$\frac{\partial^2 T}{\partial x^2} + \frac{\partial^2 T}{\partial y^2} + \frac{\partial^2 T}{\partial z^2} = \frac{1}{\kappa}\frac{\partial T}{\partial t} \qquad (2.1.1)$$

where κ is the thermal diffusivity of the medium, $\kappa = \frac{\lambda}{\rho c}$ and λ is the thermal conductivity, ρc is the specific heat per unit volume.

Using the idea that a finite quantity of heat is liberated instantaneously at a given point and time, in an infinite solid medium, i.e. the instantaneous point source of heat, the heat equation is satisfied by the following solution[22,26].

$$T = \frac{Q}{8\ (\pi\kappa t)^{3/2}} EXP\left[\frac{-\left\{(x-x')^2 + (y-y')^2 + (z-z')^2\right\}}{4\kappa t}\right] \qquad (2.1.2)$$

This solution may be interpreted as the temperature in an infinite solid medium at the point (x,y,z) due to quantity of heat $Q\ \rho C_p$ instantaneously liberated at $t = 0$ and at a point (x',y',z'). According to Carslaw and Jaeger, if instantaneous point sources of strength $Q\,r'\,d\theta'$ are distributed round the circle $r = r'$ in the plane $z' = 0$, temperature at time t at the point with the cylindrical coordinates (r, θ, z) is

$$\frac{Q\ r'}{8\ (\pi\kappa t)^{3/2}} \int_0^{2\pi} Exp\frac{-\left[r^2 + z^2 + r'^2 - 2rr'\cos(\theta-\theta')\right]}{4\kappa t} \qquad (2.1.3)$$

$$T = \frac{Q'}{8\ (\pi\kappa t)^{3/2}} Exp\left\{-\left[\frac{r^2 + r'^2 + z^2}{4\kappa t}\right]\right\}\ I_0\left(\frac{rr'}{2\kappa t}\right) \qquad (2.1.4)$$

where I_0 is the modified Bessel function, $Q' = 2\pi r' Q$, and $Q'\rho C_p$ is the total amount of heat liberated in the ring source.

If we assume a series of concentric ring source with a constant out put of power per unit length in all the ring sources, we have accordingly a temperature increase at a point r and in the plane z = 0

$$T(r,t) = \sum_{\text{all } r' \text{ values}} \frac{2\ \pi\ r'\ Q}{8\ (\pi\kappa t)^{3/2}} \text{Exp}\left\{-\frac{\left[r^2 + r'^2\right]}{4\kappa t}\right\}\ I_0\left(\frac{rr'}{2\kappa t}\right) \qquad (2.1.5)$$

Now if the output power per unit length of each of the ring sources is

$$Q\ \rho\ C_p = \phi(t)\ \rho\ C_p\ dt' \qquad (2.1.6)$$

The temperature increase at the time t and at a distance r from the origin is given by

$$\Delta T\ (r,t) = \int_0^t dt' \frac{\phi(t')}{4\ \pi^{1/2}\left[\kappa\ (t-t')\right]^{3/2}} \sum_{r'}\ r'\ \text{Exp}\left\{\frac{-\ (r^2 - r'^2)}{4\ \kappa\ (t-t')}\right\}\ I_0\left(\frac{r\ r'}{2\ \kappa\ (t-t')}\right) \qquad (2.1.7)$$

The total out put power in the set of concentric and continuous sources is assumed to be constant and can be expressed as

$$P_0 = \sum_{r'} 2\pi r'\ \phi\rho c_p \qquad (2.1.8)$$

If m is the number of concentric ring sources, and a is the radius of the largest ring, then $r'_K = K\left(\frac{a}{m}\right)$ is the radius of the source number k

$$P_0 = 2\pi\phi\rho C_p \sum_{K=1}^{m} K\frac{a}{m} = 2\pi a\phi\rho C_p \frac{1}{m}\sum_{K=1}^{m} k \qquad (2.1.9)$$

and

$$P_0 = \pi a \phi \rho C_p (m+1) = \frac{\pi a \phi \lambda (m+1)}{\kappa} \qquad (2.1.10)$$

then using Eqs.(2.1.7---10)

$$\Delta T(r,t) = \frac{P_0 \kappa}{4\pi^{3/2} m(m+1)\lambda} \int_0^t \frac{dt'}{[\kappa(t-t')]^{3/2}} \sum_{K=1}^{m} K \; Exp\left\{ -\left[\frac{r^2 + \left(k\frac{a}{m}\right)^2}{4\kappa(t-t')} \right] \right\} I_0\left(r \frac{\left(k\frac{a}{m}\right)}{2\kappa(t-t')} \right)$$

For the mathematical conveniences we define the following dimensional quantities

$$\tau = \sqrt{\frac{t}{\theta}} = \frac{\sqrt{\kappa t}}{a}; \qquad \theta = \frac{a^2}{\kappa} \quad and \quad s^2 = \frac{\kappa(t-t')}{a^2}$$

where t is the time measured from the start of three transient heating, θ is the characteristic time, and κ is the thermal diffusivity of the sample.

Then the temperature increase in the z = 0 plane at a distance r from the origin due to k concentric ring sources can be written as

$$\Delta T(r,\tau) = \frac{p_0}{2\pi^{3/2} a\lambda m(m+1)} \int_0^{\tau} \frac{ds}{s^2} \sum_{k=1}^{m} k \; Exp\left\{ -\frac{\left[\left(\frac{k}{m}\right)^2 + \left(\frac{r}{a}\right)^2 \right]}{4s^2} \right\} I_0\left(\frac{\frac{kr}{ma}}{2s^2} \right) \qquad (2.1.11)$$

If m concentric ring sources, make up the sensor and each ring source consists of a metallic ribbon with thickness 2ε ($\approx 10\mu m$) and breadth 2d ($\approx$ 0.4mm), then we get the following expression for the resistance

Resistance of the first ring source; $$R_1 = \frac{2\pi \frac{a}{m}}{2\varepsilon \cdot 2d} \rho_0 \left[1 + \alpha \Delta T\left(\frac{a}{m}, \tau \right) \right]$$

Resistance of the nth ring source $$R_n = \frac{2\pi n \frac{a}{m}}{2\varepsilon \cdot 2d} \rho_0 \left[1 + \alpha \Delta T\left(\frac{na}{m}, \tau \right) \right]$$

The total resistance of the m rings will be

$$R_{total} = \sum_{n=1}^{m} R_n$$

$$R_{Total} = \frac{2\pi\ a\ \rho_0}{2\varepsilon\ 2d}\frac{1}{m}\sum_{n=1}^{m}\left[n + \alpha n\Delta T\left(n\frac{a}{m},\tau\right)\right]$$

$$R_{Total} = \frac{2\pi\ a\ \rho_0}{2\varepsilon\ 2d}\ \frac{1}{m}\ \frac{m(m+1)}{m}\left[1+\alpha\frac{2}{m(m+1)}\sum_{n=1}^{m}n-\Delta T\left(n\frac{a}{m},\tau\right)\right]$$

Since

$$R_{Total} = R_0\left[1+\alpha\overline{\Delta T(\tau)}\right]$$

The expression outside the brackets is simply equal to the total resistance at zero temperature, where

$$\overline{\Delta T(\tau)} = \frac{2}{m(m+1)}\sum_{n=1}^{m} n\ \Delta T\left(n\frac{a}{m},\tau\right)$$

Then using Eq. (2.1.11), the mean temperature increase will be expressed

$$\overline{\Delta T(\tau)} = \sum_{n=1}^{m} n - \frac{P_0}{\pi^{3/2}a\lambda m^2(m+1)^2}\int_0^{\tau}\frac{ds}{s^2}\sum_{k=1}^{m} k\ \ Exp\left\{\frac{-\left[\left(\frac{k}{m}\right)^2+\left(\frac{n}{m}\right)^2\right]}{4s^2}\right\}\ I_0\left(\frac{\frac{k}{m}\frac{n}{m}}{2s^2}\right)$$

$$\overline{\Delta T(\tau)} = P_0(\pi^{3/2}a\lambda)^{-1}D\ (\tau) \qquad (2.1.12)$$

where

$$D(\tau) = [m(m+1)]^{-2} \int_0^{\tau} ds\ s^{-2} \left[\sum_{n=1}^{m} n \sum_{k=1}^{m} K \exp\left(\frac{-(n^2+k^2)}{4m^2 s^2} \right) I_0\left(\frac{nk}{2m^2 s^2} \right) \right] \qquad (2.1.13)$$

P_0 is the total out put power, λ is the thermal conductivity of the sample, and a is the radius of the sensor. $D(\tau)$ is the theoretical expression of the time dependent temperature increase, which describes the conducting pattern of the disk shaped sensor, assuming that the disk consists of a number m of the concentric ring sources. Fig. 2.2a

To insure the validity of the theory, the design parameters of the experiment should be chosen, and data reduction procedures should be carried out in such a way that the deviations from the ideal conditions can be justified. In order words, there are possible deviations due to experimental factors, and there are possible deviations due to improper data handling.

2.2 DEVIATION FROM THE THEORY DUE TO EXPERIMENTAL FACTORS

The possible deviation from the ideal conditions due to experimental factors can be divided into two parts: deviations due to design parameters of the sensor, and deviations due to experimental set up, all of which will be dealt as follows:

2.2.1 DEVIATIONS DUE TO DESIGN PARAMETERS OF THE SENSOR

Since the design parameters of the sensor are numerous, the discussion will be limited only to those parameters which are related to the sensor thickness, heat capacity, the effect of insulation layers and shape of the heavy electrodes. Other design parameters such as factors related to the shape of the conducting pattern, are not included in the following discussions.

2.2.2 NEGLIGIBLE THICKNESS AND HEAT CAPACITY OF THE TPS-ELEMENT

Regarding the assumption that the total output power P_0 in Eq. (2.1.12) is constant, and that all this power is transferred to and consumed for heating the sample, we can justify this assumption by making a rough estimation of the ratio between the power actually consumed by the sample and power actually required to raise the temperature of the element itself. An expression for the power dissipated in the element can be written as

$$P_e = 2\ \pi\ a^2 \upsilon \rho_e C_e \left[\frac{d(\Delta T(\tau))}{dt}\right]$$

where $\rho_e C_e$ is the total heat capacity per unit volume of three element, and $2\ \upsilon$ is its thickness, while the total power delivered to the sample is expressed as

$$P_s = 2\pi r^2\ 1\ \rho_s C_s \left[\frac{d(\Delta T(\tau))}{dt}\right]$$

where 2 I is the thickness of the heated part of the sample, and r is its radius. Considering the fact that in most of the cases, including the ones treated in this work, the ratio

$$\frac{\rho_s C_s}{\rho_e C_e} \approx 1$$

and selecting typical values for the dimension of both the sample and the element, such as $2\upsilon = 60\mu m$, a =10mm, r = 15mm and 2l =20mm, the ratio between the powers is $\leq 10^{-5}$. In other words, only less than 0.1% of the total power delivered is dissipated in the element. Furthermore ,this will disturb the recording only in the very beginning of the transient event, where it may be avoided as we will see later.

2.2.3 THE INFLUENCE OF THE INSULATING LAYER

The influence of the insulation on the function of the element as a perfect heater might be due to the effect of either the insulation between the different parts of

the pattern (between the bifilar spirals) in the radial direction or the insulation covering the pattern on both sides in the vertical direction. However the effect of the former is larger than the effect of the later, due to the smaller contact area between the metallic pattern and insulation. The characteristic time of the insulation is expressed as

$$\theta_i = \frac{\delta^2}{\kappa_i}$$

where κ_i is the thermal diffusivity of the insulation, and 2δ is the largest lateral distance between two conducting spirals in the pattern. Similarly the characteristic time of the sample is expressed as

$$\theta_s = \frac{r^2}{\kappa_s}$$

Thus the influence of the insulation can be avoided if we have

$$\theta_s >> \theta_i$$

a condition which is not difficult to fulfill [27]. For instance, using the typical values $\delta \approx 0.2$ mm and $\kappa \approx$ 0.1 mm/sec gives $\theta_i \approx$ 0.4sec, to compared with typical value of $\theta_s \approx$ 100 sec.

2.2.4 NEGLECTING THE HEAT LEAK THROUGH THE HEAVY ELECTRODES

The rate of the heat losses through the flat portion of the element Fig. 2.2a can be estimated as

$$P_l = \lambda_m A_l \left(\frac{dT}{dx}\right)$$

where x is the distance between the soldering point of the copper wire and the heating spiral, λ_m is the thermal conductivity of the metal from which the sensor is

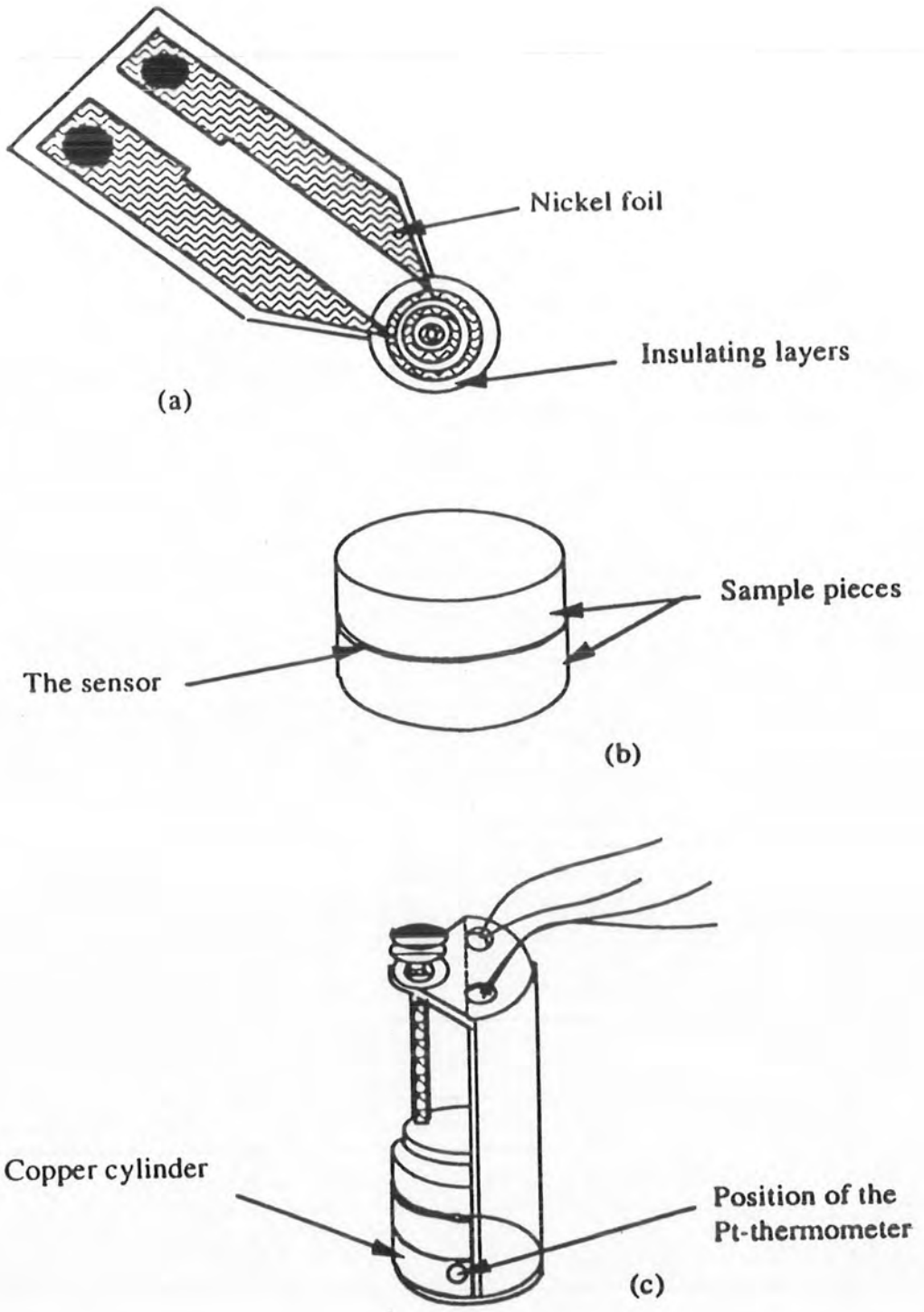

Figure 2.2 (a) The TPS-element, (b) The shape of the sample, (c) The sample arrangement in the sample holder.

made, and A_1 is the cross-sectional area of the electrodes. At the end of the experiment, we can estimate the total power supplied as

$$P = R_0 I^2$$

where I ($\approx$ 300 mA) is the current pulse. For a typical temperature increase of dT $\approx$ 1K and typical values such as $\lambda_m \approx 70$ W/mK for nickel, $A_1 \approx 10^{-7}$ and x $\approx$ 20mm, the maximum rate of heat losses at the end of the experiment becomes less than 0.1% of the total power delivered.

2.3 DEVIATIONS DUE TO EXPERIMENTAL SET- UP

The experimental set up includes the arrangement of the sample, the basic electrical circuit and sort of leads used.

2.3.1 ARRANGEMENT OF THE SAMPLE

There are two aspects to be considered in the arrangement of the samples. Firstly, we must insure a good thermal contact between the sensor and the sample pieces, which is done by clamping the TPS-element between the sample halves via a screw arrangement Fig. 2.2c

Secondly, in some cases it might be necessary to place (guarding) the sample pieces and the sensor arrangement inside the copper cylinder in order to protect the sample from the external radiation or/and to achieve a homogeneous temperature distribution around the sample.

2.3.2 THE BASIC CIRCUIT DESIGN

The essential components of the electrical circuit were a constant power supply, a resistance R_p and a bridge arrangement. The assumption that we have a constant power supply can be justified as follow: Firstly, from the experimental side by choosing the proper circuit design based on a constant voltage input, and working in a slightly varying current mode. For example, we can use a Wheatstone bridge Fig. 2.3

The use of bridge increases the sensitivity of the measurement and make it less dependent on the fluctuations of the current in the circuit. The total resistance of the bridge arms having the ratio of 1:100 to keep the current constant within 1 %

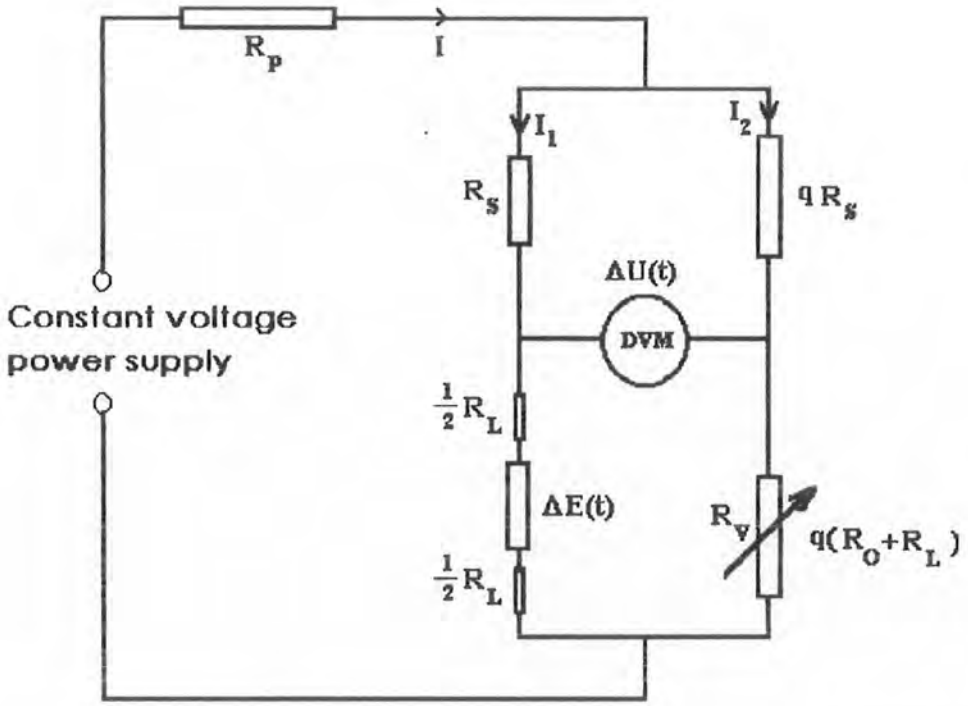

Fig. 2.3 The electrical bridge circuit used to monitor the voltage $\Delta U(t)$ **variation across the bridge via the digital voltmeter DVM.**

outside the bridge and to insure that 99 % of the current pulse is passing to the sensor i.e.

$$I_1 = \left[\frac{q}{(q+1)}\right] I$$

where q=100 is the ratio between the resistance of the two arms of the bridge. The standard resistance was used to monitor the current through the heater. The electrical recording was made with a digital multimeter (HP 3478A) on-line to a microcomputer. Secondly, from the theoretical side, by using the time correction t_c(see section 2.4 point(2)) which is defined as the time delay that hinders the current pulse to rise to a constant level in the very beginning of the experiment. This

time correction is affected by the intrinsic time delay of the different pieces of the equipment (computer, power supply etc.) used in connection with the electrical circuit.

2.3.3 EFFECT OF OTHER CIRCUIT COMPONENTS

The aim is to monitor the voltage (resistance) variation across the sensor. However, in practice the voltage variations across the bridge are monitored, and that involves also other resistors beside the designed circuit Fig. 2.3. All of which might effect the recorded variations. Hence to account for such affects, a theoretical analysis is essential to justify the assumptions imposed on the design of the bridge circuit.

The bridge is first operated in balanced mode by making U_{in} small enough to that a small current flows through the non-linear resistor $R_0(\approx 3.67\Omega)$, which is the initial resistance of the TPS-element before passing any current, such that the temperature increase in R_0 is negligible. Then R_V is adjusted such that the potential difference across a and b is zero. Under this condition we get the following condition

$$\frac{R_1(=qR_s)}{R_S} = \frac{R_2(=R_v)}{R_0} = q$$

Based on a constant voltage input, we can start with the following expressions for the voltage variations across the TPS- element ΔE and the total voltage V_{inp} across the left arm of the bridge is;

$$\Delta E(t) = \left(I_1 - \Delta I_1\right)\left(R_0 + \Delta R\right)$$

$$V_{inp} = I_1\left(R_S + R_0 + R_L\right)$$

Where $R_s\left(\approx 1\Omega\right)$ is the standard resistance with current rating much higher than I_1. The resultant $\Delta E(t)$ can be calculated as follow :

The bridge is then switched over to the unbalanced mode with U_{in} such that a large enough current flows through R_0 (TPS-element) so as to give a temperature increase of about 1K with U_{in} voltage across the bridge, We get

$$\left(I_1 - \Delta I_1\right)\left(R_\ell + \Delta R\right) = \left(I_2 + \Delta I_2\right)\, q\, R_\ell$$

Where $$R_\ell = \left(R_s + R_0 + R_L\right)$$

Using $$I_1\left(R_s + R_0 + R_L\right) = q\, I_2\left(R_s + R_0 + R_L\right)$$

and assuming $$\Delta I_1\, \Delta R \cong 0, \quad I_1 = q\, I_2$$

We have $$I_1 \Delta R = R_\ell\, \Delta I_1 + qR_\ell\, \Delta I_2 + \Delta I_1 \Delta R$$

The input voltage can be expressed as

$$U_{in} = R_p\left(I_1 + I_2 - \Delta I_1 + \Delta I_2\right) + \left(I_2 + \Delta I_2\right) q\, R_\ell \approx \text{cos tt.}$$

Since U_{in} is constant, we can write

$$q\, R_\ell\, \Delta I_2 - R_p\left(\Delta I_1 - \Delta I_2\right) = 0$$

$$\Delta I_2 = \Delta I_1\left(\frac{R_p}{q\, R_\ell + R_p}\right)$$

Similarly

$$\frac{\Delta I_2}{I_2} = \frac{\Delta I_1}{I_1}\left[\frac{q\, R_p}{q\, R_\ell + R_p}\right]$$

Now $$\Delta R = R_\ell\, \frac{\Delta I_1}{I_1} + qR_\ell\, \frac{\Delta I_2}{I_1} + \Delta R\, \frac{\Delta I_1}{I_1}$$

$$\frac{\Delta R}{R_\ell} = \frac{\Delta I_1}{I_1} + \frac{\Delta R}{R_\ell}\, \frac{\Delta I_1}{I_1} + \frac{\Delta I_2}{I_2}$$

$$\frac{\Delta R}{R_\ell} = \frac{\Delta I_1}{I_1} + \frac{\Delta R}{R_\ell}\ \frac{\Delta I_1}{I_1} + \frac{\Delta I_1}{I_1}\left(\frac{q\ R_p}{q\ R_\ell + R_p}\right)$$

$$\frac{\Delta R}{R_\ell}\left(1 - \frac{\Delta I_1}{I_1}\right) = \frac{\Delta I_1}{I_1}\left(1 + \frac{q\ R_p}{q\ R_\ell + R_p}\right)$$

$$\frac{\Delta R}{R_\ell}\left(1 - \frac{\Delta I_1}{I_1}\right) = a\ \frac{\Delta I_1}{I_1} \qquad (2.3.1)$$

where $$a = 1 + \frac{q\ R_p}{q\ R_\ell + R_p}$$

with $$x = \frac{\Delta R}{R_\ell}$$

$$\frac{\Delta I_2}{I_2} = \frac{\Delta I_1}{I_1}(a - 1)$$

Thus above Eq.(2.3.1) becomes

$$x\left(1 + \frac{\Delta I_1}{I_1}\right) = a\frac{\Delta I_1}{I_1}$$

$$\frac{\Delta I_1}{I_1} = \left(\frac{x}{x + a}\right)$$

Similarly $$\frac{\Delta I_2}{I_2} = \frac{x}{x + a}(a - 1)$$

The voltage developed across the terminal a and b due to the change in the resistance of the TPS-element R_0 is given by[29].

$$\Delta U(t) = \left(I_1 - \Delta I_1\right)\left(R_0 + \Delta R\right) - \left(I_2 + \Delta I_2\right)\ q\ R_0$$

$$= \left(I_1 - \Delta I_1\right)\left(R_\ell - R_s + \Delta R\right) - \left(I_2 + \Delta I_2\right)\ q\ \left(R_\ell - R_s\right)$$

$$= \Delta R\left(1-\frac{x}{x+a}\right)-\left(R_{\ell}-R_{s}\right)\left(\frac{x}{x+a}+\frac{ax-x}{x+a}\right)$$

Simplifying We have the equation

$$\frac{\Delta U(t)}{a\ I_1} = \frac{\Delta R - \ xR_{\ell}\ + \ xR_{s}}{x+a}$$

$$\frac{\Delta U(t)}{R_s a\ I_1} = \frac{x}{x+a}$$

Let

$$P = \frac{x}{x+a}$$

Where $$P = \frac{\Delta U(t)}{a\ I_1 R_s}$$

or $$\frac{Pa}{1-P} = x \qquad (2.3.2)$$

Substitution to original variables in the above Eq.(2.3.2), We get

$$\frac{\left[\frac{\Delta U(t)}{I_1 R_s}\right]}{\left[\ 1-\frac{\Delta U(t)}{aI_1 R_s}\ \right]} = \frac{\Delta R}{R_{\ell}}$$

where $$\Delta R = \alpha\ R_0\ \Delta T$$

$$\frac{\Delta U(t)}{I_1 R_s\left(1-\frac{\Delta U(t)}{a\ I_1 R_s}\right)} = \frac{\Delta R}{R_{\ell}}$$

The relation between the voltage change across the TPS-element, $\Delta E(t)$ and the measured voltage across the bridge, $\Delta U(t)$ in the off-balance bridge is given by

$$\Delta E(t) = \frac{\Delta U(t)}{1 - \dfrac{\Delta U(t)}{a\ \bar{I}_1\ R_s}}$$

$$\Delta E(t) = \Delta U(t) \left[1 - \frac{\Delta U(t)}{K\ I_1 R_s} \right]^{-1} \qquad (2.3.3)$$

Where

$$K = 1 + \left\{ \frac{q\ R_p}{\left[q\ \left(R_s + R_0 + R_L \right) + R_p \right]} \right\} \qquad (2.3.4)$$

and $R_p (\approx 0.05)$ is the effective resistance of the remaining wires in the circuit outside the arms of the bridge.

2.3.4 THE LEADS RESISTANCE R_L

In cases when long leads are needed, for instance, for measurements at low temperature inside a cryostat [20] or for high temperature measurements inside an oven [29]. Care must be taken to eliminate any heating effects due to these leads which might occur outside the heating element/sensor. During the passage of the current pulse, four leads are used to measure R_0 prior to the transient recording.

The resistance of the leads R_L is determined from the difference between R_0 and the values of the variable resistance R_V Fig. 2.3. This is done directly after balancing the bridge, and before passing the current pulse that is heating the sensor/sample assembly. To compensate for this effect theoretically, R_L has been included in the expression describing the voltage variations across the bridge, see Eq. (2.3.3) and Eq. (2.3.4).

2.4 DEVIATION FROM THE THEORY DUE TO IMPROPER DATA REDUCTION

The data reduction procedures should be carried out in such a way that any possible deviation from the theoretical equations can be avoided. These reduction

procedures involve obtaining the best theoretical representation data which include the following:

2.4.1 EVALUATION OF THE INTEGRAL EQUATION OF THE SENSOR

It is a quite difficult task to obtain an exact solution to describe and satisfy the actual bispiral pattern of the sensor. However, from our experience, approximating the solution by concentric rings Eq. (2.1.12) did not effect the obtained results, and good accuracy can be achieved for values of τ greater than 0.06 but less than 3. The integral equation is evaluated by dividing the interval $0.06 < \tau < 3$ into sub-intervals (meshes), and then using the cubic spleen procedures to interpolate the numerically evaluated $D(\tau)$ for each desired value of τ within the specific mesh. It should be noted that, due to the mathematical nature of the expression inside the integral, it can be cumbersome to evaluate the theoretical expression of $D(\tau)$ for very small values of τ.

2.4.2 COMPENSATING FOR THE TIME DELAY

Satisfying the condition $\theta_s >> \theta_i$ implies that we can ignore the time correction in many cases. This time correction is a combination of the time delay due to the influence from the insulating layers, including the contact resistance, and/or the influence of the time delay of the equipment used in connection to the electrical circuit. However, in some cases we have to account for this time delay, and this is simply done by replacing τ by

$$\tau_c = \left[\frac{(t - t_c)}{\theta}\right]^{1/2}$$

in the relevant equations. A detailed treatment was given in 1986 for the hot-strip method by Gustafsson et al. [32].

2.4.3 COMPENSATING FOR THE TEMPERATURE DRIFT

There are cases where it might be difficult to achieve a homogeneous temperature distribution around the sample due to a temperature drift Fig. 2.4.

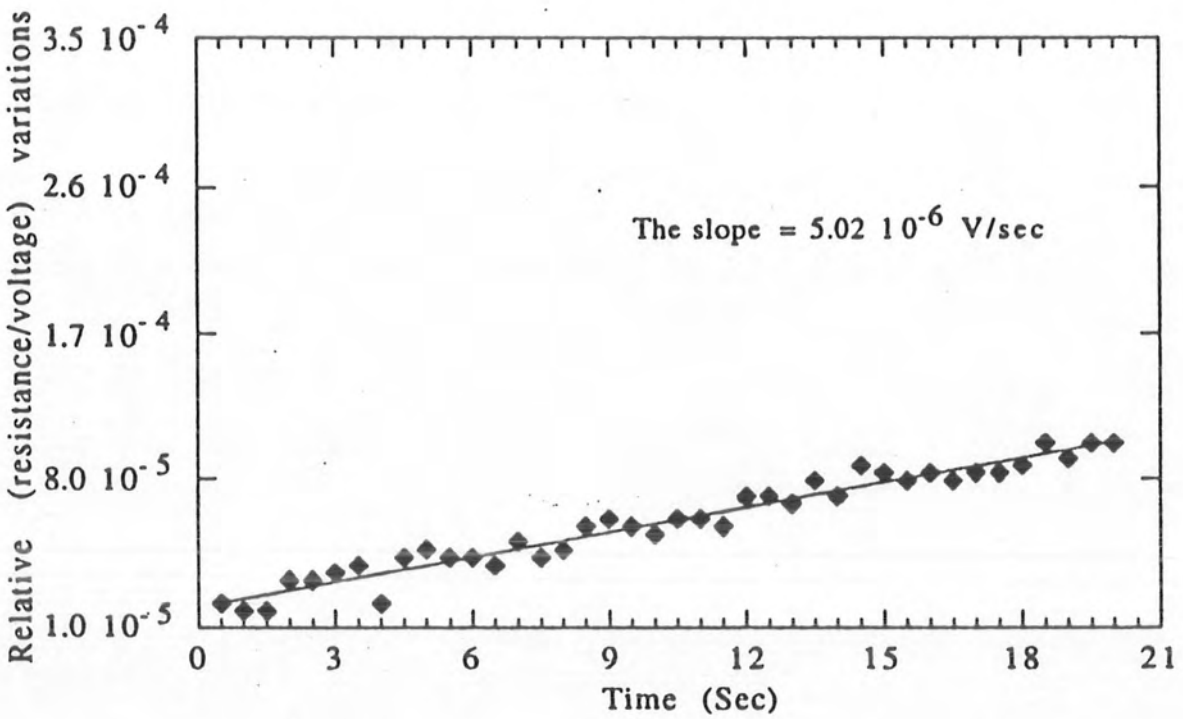

Fig. 2.4 A typical temperature drifting curve, the line is a least square fit to the corresponding data.

ISSN: 0022-3727
Volume 25 • Number 4 • 14 April 1992

JOURNAL OF PHYSICS D

APPLIED PHYSICS

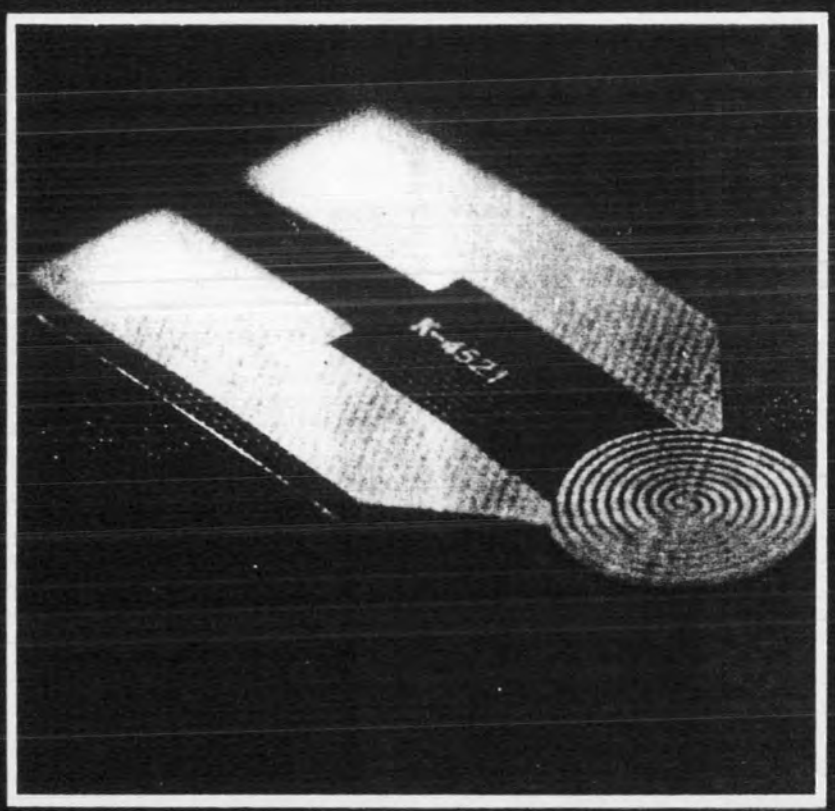

Institute of Physics Publishing
Recognized by the European Physical Society

Fig. 2.5 TPS-element

of the whole assembly (the sensor and sample pieces). In such cases the measured data are handled in order to get the actual value of the voltage variation across the TPS-element $\left(\Delta E_a(t)\right)$ as follows: Prior to the transient event, the resistance of the element is measured using the standard dc four-probe method with a measuring current of ≈10 mA for a short period of time $t_d\left(\approx 20 \text{ sec}\right)$. Then by using a least squares fit the measured data are fitted to a straight line, the slope of which gives the rate of resistance (voltage) variation of the element due to this temperature drift. Immediately after that, the experiment is performed, and the resulting $\Delta E(t)$ is multiplied by the slope of the drift line in order to get $\Delta E_d(t)$. Then the actual $\Delta E_a(t)$ is obtained by subtracting the drifted value from $\Delta E(t)$, i.e.

$$\Delta E_a(t) = \Delta E(t) - \Delta E_d(t)$$

To proceed in the calculation the actual $\Delta E_a(t)$ is used instead of the $\Delta E(t)$ in the relevant equations.

2.5 EXPERIMENTAL SET-UP AND CALIBRATION MEASUREMENTS

2.5.1 EXPERIMENTAL APPARATUS

The experimental apparatus consists of bridge circuit Fig. 2.3 and includes the following instruments for measurements.

The TPS-method uses a "resistive element" , the TPS-element/sensor, both as heat source and temperature sensor. There are a variety of configurations for different sensors such as disk, square, etc., (see Fig. 2.2a, 2.5). The question which configuration is most convenient depends on many factors such as material type, sample size, kind of leads used, etc. Fig. 2.5.

We will here limit the discussion to the disk shaped pattern, "hot disk", which has been used to collect all data reported in this work. This sensor is made of nickel

foil in the form of a bifilar spiral covered on both sides with an insulating layer of Kapton Fig. 2.2a. The thickness of the foil and the Kapton layer are 10 and 25μm, respectively, the effective diameter of the bifilar spiral is 20 mm, and the diameter of the Kapton layer is 25mm. In the experimental arrangement, Fig. 2.2b, the sensor is pressed between the sample halves which usually are two identical cylinder-shaped pieces, having a diameter of 28mm and a thickness of 10mm. Details about the specific characteristics and the design requirements of these sensors are given by Gustafsson [29].

The experiment requires an ideal constant current power supply source. However, it is not possible to have a 100% constant current due to many circuit components including (i) length of wires (ii) limiting resistance (iii) internal resistance of the measuring instruments. It was possible to have nearly constant current up to 1mA from a power supply capable of handling a constant current up to 0-2 amp/0-50V,100 W. HP 6633A System DC Power Supply was used without any heating or load current fall.

All the resistors (standard resistors Type 2792 YEW 1Ω,100Ω and decade resistors D 05, D 15 era, Holland) used in the experiment were of power type which were capable of handling current values double to that required in the experiment. There was no significant change in their resistance due to their temperature dependent coefficient of resistivity during the current flow through them. This requires that the resistors used must have a very small temperature dependent resistivity coefficient because any change in their resistance can change the magnitude of current through the circuit.

The voltages changes across the TPS-element were recorded using a digital multimeter (HP 3478A) providing an accuracy upto (0.1μV). The voltage variations (≈ 8 readings/sec) across the bridge were monitored using a digital multimeter (HP 3478A) having accuracy 0.1μV via an unbalanced mode of the bridge circuit.

In order to obtain the required information with reasonable accuracy, it is essential that the time period for collecting the data should be of the same order as that of the characteristic time $\theta = \frac{a^2}{\kappa}$ sec. [see section 2.1.1]. This requires fast recording and measuring instrument. So a computer 486 (SCANDIC PERSONDATORER)with fast switching, rise and fall time was used in the experiment.

2.5.2 LOW TEMPERATURE MEASUREMENTS

The experimental apparatus for measurements at low temperature consists of the room temperature apparatus (the bridge circuit, power supply, computer.. etc.), and the following additions:

A total of eight Ag coated low resistance leads(diameter $\approx$ 0.5 mm and length $\approx$ 1.o m) were used to measure the temperature and to deliver the current to the sensor. During the passage of the current pulse, four of these leads were used to reduce Joule heating effects which might occur outside the heating element/sensor. Rest of the four leads were connected to a Pt-100 thermometer placed very close to the sample that was used to determine the temperature of the surroundings of the specimen (see Fig.2.2c). The resistance variations in this thermometer were recorded by Keithley 195A digital multimeter which can read the variation in resistance upto 0.1mΩ. The Pt-100 thermometer was calibrated before use. The calibration process was done in the following way.

Platinum resistance thermometer with the connecting wires was first dipped into the liquid nitrogen (of known temperature i.e., 77K). The outer terminals of the thermometer were connected to a digital ohm meter. Since platinum resistance thermometer has a temperature dependent resistance, so observations of the resistance were recorded at liquid nitrogen temperature. The thermometer was then dipped along with a Celsius thermometer into cold ice water and the temperature as well as the corresponding resistance were noted. The temperature recorded from

thermometer was in Celsius scale, so it was converted into Kelvin scale using the relation

$$K = {}^{0}C + 273$$

Other few readings were observed at room temperature and few degrees above the room temperature by heating the water. Then a graph in Fig. 2.6 was plotted between these resistances and the corresponding temperatures which is shown here.

From this graph, values of resistance (Ω) corresponding to different temperatures (Kelvin) were noted. The calibration table so formed is given in the table(Appendix 2). The calibration curve was often checked during the course of experiment. The temperature variation was within ±1K.

Cryostat is an instrument with the help of which a specified low temperature can be maintained. Since thermal conductivity of the superconducting materials is temperature dependent, so in order to see the effect of temperature on thermal conductivity, an arrangement was required for changing the temperature of the material with time.

Our simple cryostat consists of (i) a liquid nitrogen dewar (ii) one end closed hollow stainless steel cylinder (iii) a dipstick(graduated stainless steel pipe) attached with the sample holder assembly. Fig.2.10.

Our liquid nitrogen dewar has a capacity of containing about 25 liters of liquid nitrogen. There are no chances of liquid nitrogen leakage from any point except from the cover, at the container, due to the diffusion and then evaporation from it. The diameter of the opening of container is about 6.3cm.

One end closed hollow cylinder prevents the sample assembly from a direct contact with the liquid nitrogen, which may cause a damage to the circuit. It has a length of about 55.5 cm and a diameter of about 4.0 cm. It can be inserted directly into the liquid nitrogen container. At the open end, a disc of 7.5 cm outer diameter,

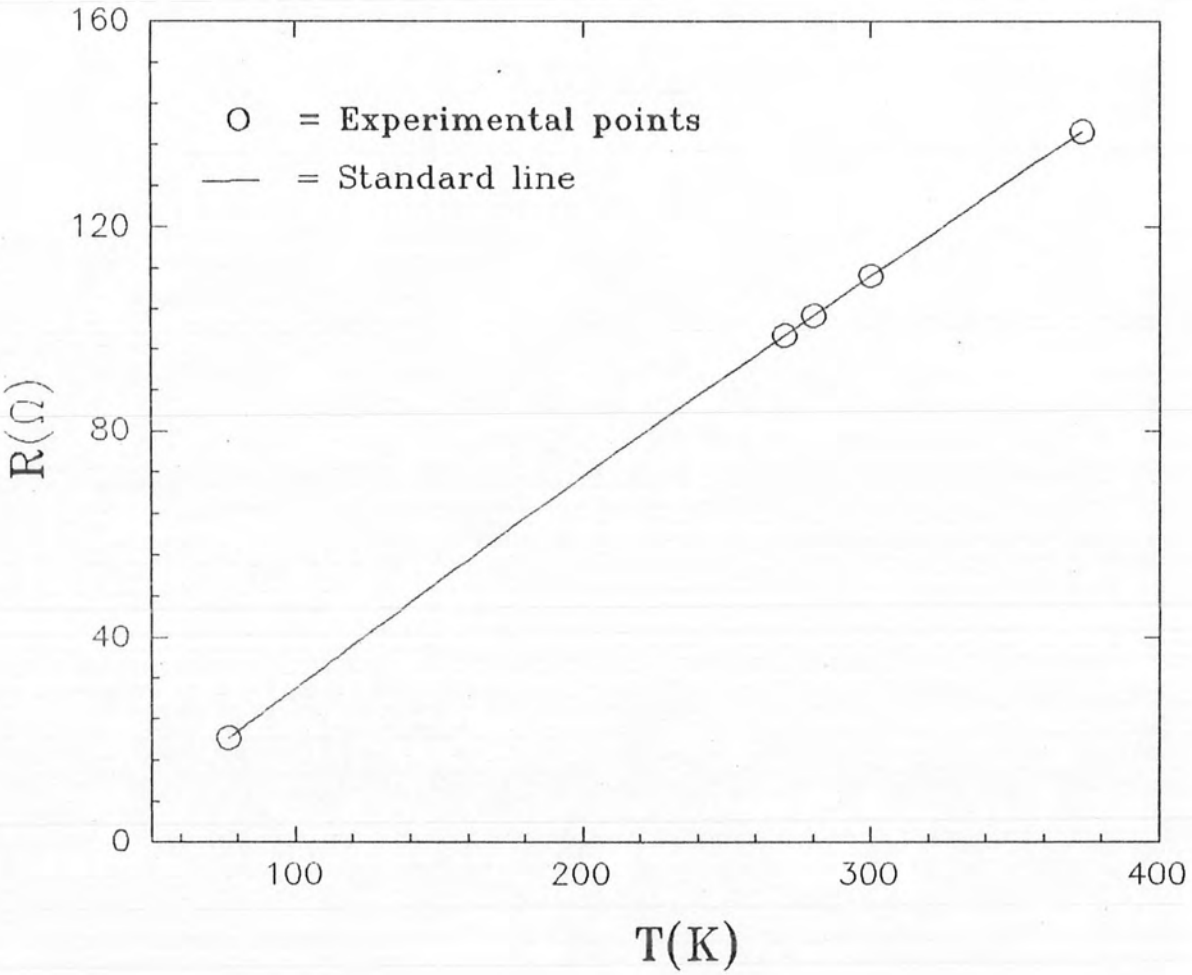

Fig. 2.6 Calibrated platinum resistance (Pt−100) thermometer analogue

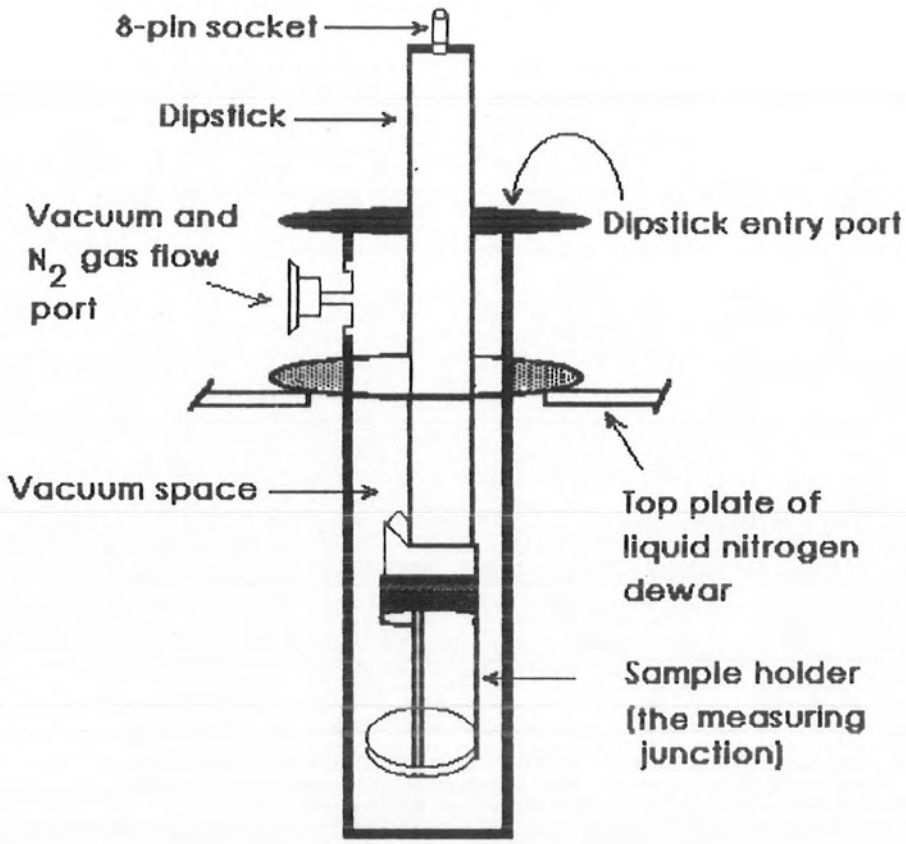

Fig.2.10 Block diagram of the cryostat

having a central hole with a diameter comparable to that of the cylinder is fitted which prevents the cylinder from falling into the liquid dewar. A stopping valve with two ports is also attached with the cylinder, from where an evacuation and nitrogen gas flow is made inside the cylinder. The temperature gradient is achieved by the successive sliding of the cylinder inside the liquid nitrogen container. A rotary vane pump, which can produce a pressure down to 10^{-2} to 10^{-3} atm linkd with a commonly used Edward's Pirani 501 guage(measuring range from 1 mbar to 5×10^{-3} mbar) for measuring the pressure, was fitted with the pumping system.

A dipstick (graduated stainless steel pipe) of length 60 cm and diameter 2.7cm is holding the sample holder assembly at its one end, while at the other end, a circular stainless steel disc of diameter 5.5 cm with a central hole comparable to that of the diameter of the dipstick is attached with the dipstick, which is not only holding the dipstick along with the sample holder assembly inside the holllow cylinder, but also makes the system inside the cylinder air tight (Since the disc has an O ring which helps the dipstick to fit tightly with the cylinder). All the wires are passed through this dipstick, which are used for making connections with temperature recording instrument, power supply and the voltage measuring instrument through a multipin socket, attached at its upper end.

The sample holder assembly is a necessary part of this arrangement for thermal conductivity measurements. The shape of the sample holder is shown in Fig. 2.2c. The sample holder assembly is attached with the dip stick with the help of grooves made on the outer and inner surfaces of sample holder and dip stick respectively. There are concentric cylindrical holes through the cylindrical portion of the holder to pass wires through it with a central hole for a screw to provide any further tightening if required to adjust the position of the samples under observation. A block diagram of the equipment used is shown in Fig. 2.7.

In addition to the common procedures when performing measurements at room temperature, the TCR values at different temperatures were obtained by differentiating the resistance equation found from the fitting during the calibration procedures as follows :

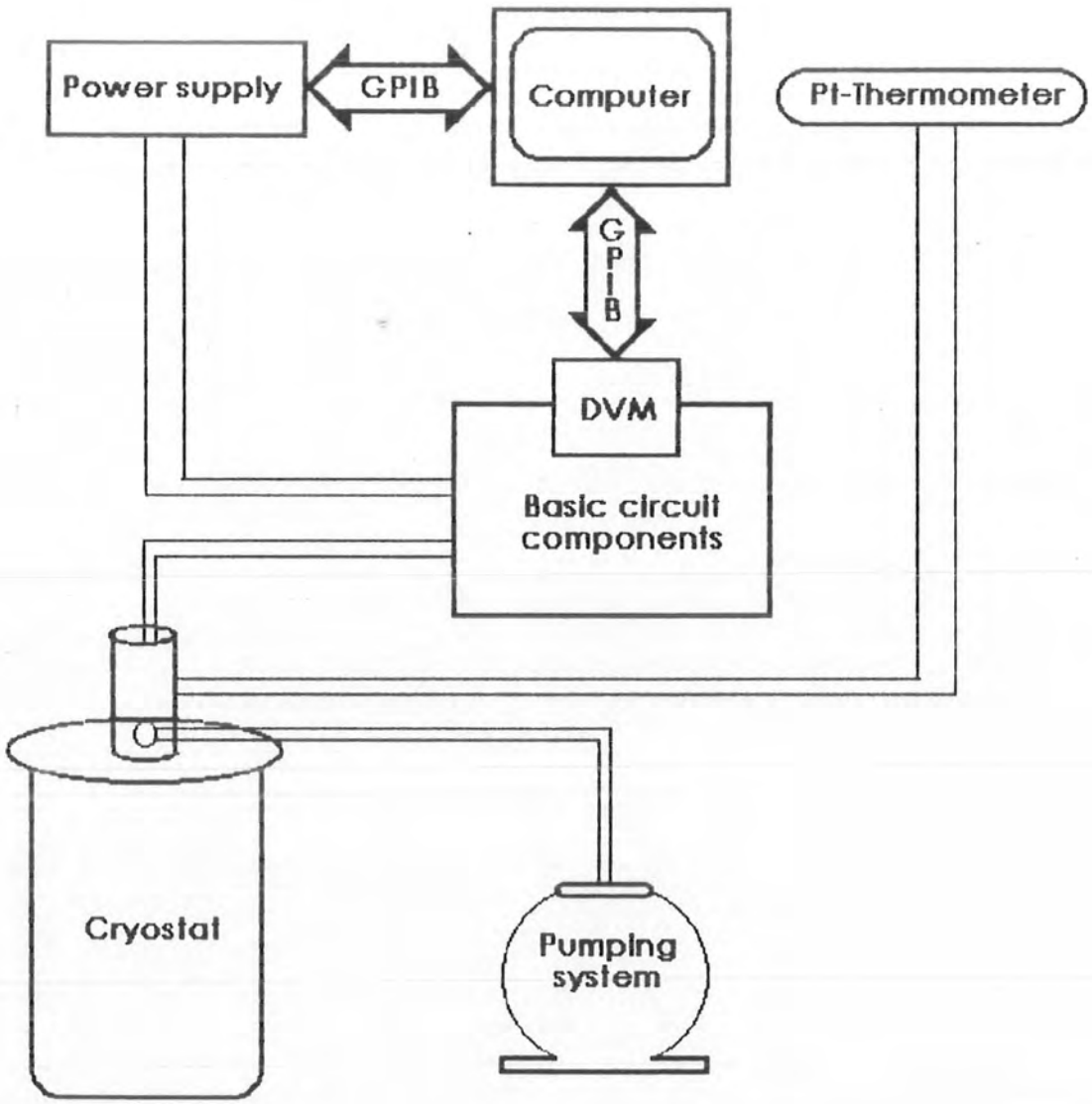

Fig. 2.7 Block diagram of the experimental setup at low temperature, where DVM is a digital voltmeter and GPIB is a general purpose interface bus.

2.5.3 TEMPERATURE COEFFICIENT OF RESISTIVITY OF THE TPS-ELEMENT

For metals in general, it is easy to have a good fit to a theoretical equation for the measured resistivity as a function of temperature. For example in case of nickel there is a good fit of the resistivity for the temperature range (77-300K).

Since the temperature coefficient of resistivity α (The change in resistance of the material per unit resistance per degree rise in temperature, its unit is K^{-1}) can be calculated by differentiating the fitted resistivity equation with respect to the temperature. Also the voltage changes are directly affected by TCR(α) as is obvious from equation (2.1.12) so it was necessary to determine this coefficient. so the TCR values are obtained by evaluating the derivative at the particular temperature of interest.

To obtain a reliable equation for the measured resistance of the TPS-element , covering the whole temperature range of interest (77-373K) the measured data were fitted to the following forth order polynomial

$$R(T) = A + BT + CT^2 + DT^3 + ET^4 \qquad (2.5.1)$$

where the values of the constants are given in the table (2.1).
The reliability of the fitting has been judged by the obtained value of the regression coefficient, r = 0.99999
Using Eq.(2.5.1) and the definition of α, the TCR values can be obtained from

$$\alpha(T) = \frac{B + 2CT + 3DT^2 + 4ET^3}{A + BT + CT^2 + DT^3 + ET^4} \qquad (2.5.2)$$

The data and the fitted polynomial are shown in Fig. 2.8a, 2.8b .
Appendix I shows typical values of R(T) and α(T) as obtained by using Eq's (2.5.1) and (2.5.2) for the TPS-element

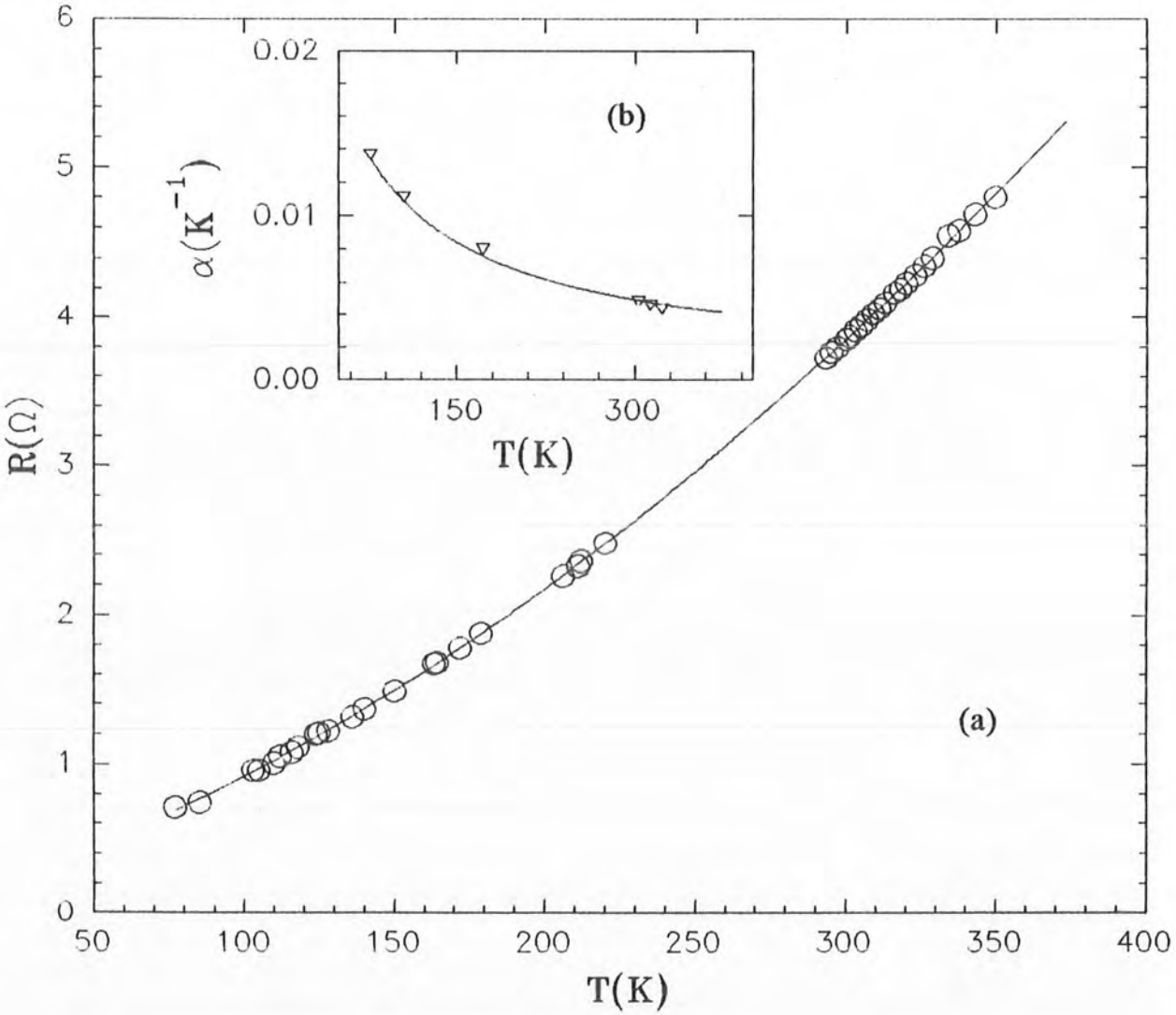

Fig. 2.8a The resistance of the TPS- element as a function of temperature fitted to Eq. (1).

2.8b A plot of α Vs T for the TPS-element, ∇ represents the experimental points, (—) shows the fitted curve to the forth order polynomial.

Table: 2.1 Parameters from the fit of Eq. (2.5.1)

Parameter	Value	Units
A	0.2896	Ω
B	-0.001438	ΩK^{-1}
C	5.815	$10^{-5}\ \Omega K^{-2}$
D	1.118	$10^{-7}\ \Omega K^{-3}$
E	1.138	$10^{-10}\ \Omega K^{-4}$

Experimentally the temperature coefficient of Kapton insulated TPS-element was determined as follow: In the first, the TPS-element was subjected to room temperature and its resistance and respective temperature were noted subsequently by four-wire method using Philips PM 2535 type multimeter. Silver wires were used as connecting leads to TPS-element. Then the whole arrangement was placed in ice water at a lower temperature and then at some higher temperatures. The TCR was calculated using the formula

$$\alpha = \frac{R_2 - R_1}{R_1(T_2 - T_1)} \qquad (2.5.3)$$

Where, R_1=Resistance of TPS-element at low temperature.

R_2=Resistance of TPS-element at high temperature.

T_1 = Lower temperature of the TPS-element.

T_2 = High temperature of TPS-element.

TCR was calculated by using the Eq. (2.5.3). Experimental and theoretical values of TCR versus temperature are plotted. Fig.2.8b,

2.5.4 PRECAUTIONS

Furthermore the following precautions were considered when performing the experiment.

(i) The sample space is evacuated down to $10^{-1} - 10^{-2}$ mbar prior to performing any measurements using the pumping system because it is our aim to attain the vacuum condition which is sufficient for conduction purpose.

(ii) To be consistent with the total time, the system needs to be at saturation condition. No successive measurements were taken with less intervals than the estimated time constant (around four hours) so that the sample may regain its equilibrium condition. If one keeps this time interval less than the stated value the time voltage curve will not be of steady state form due to existing non-equilibrium interactions. Also the probing depth is very small which does not contain sufficient informations about the properties of the material.

(iii) The power to heat the TPS-element was kept very low ($\approx$ 1 watt) so that the temperature increase of the sample would not exceed 1 K .

(iv) All measurements were performed under atmospheric pressure of N_2 gas introduced via the gas flow port before taking the reading very first time at the lowest temperature to facilitate the conduction.

(v) The portion of the leads reaching the sample holder inside the cryostat was kept at low temperature at all times to avoid any heating effects, which might disturb the measurements.

2.5.5 CALIBRATION MEASUREMENTS

Calibration is both a condition and a process. In the first case, calibration is the condition of an electronic instrument when its output or response is as close as possible to the specified value. In the second case of definition, calibration is a process of examination. To calibrate an instrument means to determine how close to the true value its indication or output really is. This process also include the correction and/or documentation of degree of error.

Calibration measurement is essentially a comparison of any given quantity with another quantity of the same kind chosen as a standard or a unit. Two fundamental ways can be envisioned for the comparison of the unknown quantity with a standard. In the first, a standard is always present and employed in the work, serving as a means of direct comparison. In the other, a standard is solely used for calibration and testing. This is consecutive comparison by calibration and naturally applies to direct-reading instruments. Here we come to another aspect of delineation- the manner in which the physical experiment is conducted. Again our examination will be limited to the bridge and potentiometer methods.

By the bridge method is meant the measurement (or reduction to zero) of the difference between two voltage drops produced by a single source across an electrical circuit consisting of at least two parallel branches. In this case, at balance (or quasi-balance) the indication is independent of the supply voltage.

By the potentiometer method is meant the measurement (or reduction to zero) of the difference between two independent voltage drop due to different sources. In this case, the indication, even at balance, is dependent on supply voltage. For the reason that the bridge circuit has only one source of supply, it is suitable for the measurement of circuit constants and also of current and voltages on the basis of functional relationships between them and circuit constants. The potentiometer method, on account of its character, can be employed for the direct measurement of electromotive forces, voltages and currents and for the indirect measurements of circuit constants.

EXPERIMENTAL PROCEDURE

CALIBRATION OF THE APPARATUS

The TPS-element (Sensor) is placed inside the sample halves and clamped to insure good thermal contact. Prior to the start of the measuring procedure the system is expected to in equilibrium. Since the TPS-element (Hot disc) configuration was

used in this work. They were made of 10μm thick nickel foil with insulation on each side of the metal pattern made of 25μm thick Kapton.

In experiments with insulating layers of such thickness it is necessary to delete the voltage recordings during the first few seconds because of the influence of the insulating layers. Due to the size of the heated area of the TPS-element the characteristic time of the experiment is so long that it is possible to delete a few seconds of recorded voltage values and still get very good results. No influence could be recorded from the electrical connections which have the same thickness as the metal pattern of the TPS-element. This observation is based on comparisons between the theoretical and actually recorded temperature variations.

An important aspect of the design of any TPS-element is that the pattern should be such that as large a part of the hot area as possible should be covered by the electrically conducting pattern as long as there is good insulation between the different parts of the conducting pattern. This is particularly important when insulating layers are covering the conducting pattern. Comparing with Eq. $\tau_2 = \sqrt{\frac{t}{\theta_2}}$, (θ_2 called the characteristic time, is defined as $\theta_2 = \frac{d^2}{\kappa_2}$) ,this design rule can be expressed as:

$$\frac{d^2}{\kappa_i} = \frac{a^2}{\kappa}$$

where 2d is the largest distance between two conducting strips in the pattern, and κ_i is the thermal diffusivity of the material filling out the space between the conducting strips. With 2a the overall lateral size of the hot area and κ the thermal diffusivity of the material under study, this design criterion is normally not difficult to meet. The total time of the transient recording is of the order of

$$\theta = \frac{a}{\kappa}$$

and the disturbances due to the openings in the conducting pattern would be relaxing and disappearing very quickly at the beginning of the transient event. This is the reason why the solutions of the thermal conductivity equation, proposed in the

theoretical section on the hot disc, so very closely approximate the exact solutions. A typical experimental thermogram for this type of arrangement is given in the Fig. 2.1. For evaluating the thermal properties of the sample Eq.(2.1.12) to Eq.(2.1.13) may be used in the case of hot disc, for times $\theta < t < t_{max}$. The thermal diffusivity κ is obtained by iterating such a value of θ that adjustment of , $D(\tau)$ in accordance to equation

$$\overline{\Delta T(\tau)} = \frac{P_0}{4\sqrt{\pi}\ a\lambda} H(\tau)$$

where

$$H(\tau) = \int_0^{\tau} d\upsilon \left[\text{erf}\ \ \upsilon^{-1} - \frac{\upsilon}{\sqrt{\pi}} \left\{ 1 - \exp(-\upsilon^{-2}) \right\} \right]^2 \quad \text{with} \quad \text{erf}(x) = \frac{2}{\pi} \int_0^{x} d\upsilon \quad \exp(-\upsilon^2)$$

[$H(\tau)$ function can be analytically approximated for small τ values, while for τ values larger than, say, 0.3 it has to be evaluated numerically, which is readily done with a microcomputer]. and Eq. (2.1.13) respectively gives a straight line. From the slope of this line the thermal conductivity λ of the sample is obtained.

Furthermore, in order to demonstrate that the TPS method employing this experimental setup can be used down to liquid nitrogen temperature, measurements on fused quartz samples were performed. The choice of fused quartz is due to the fact that thermal conductivity data of this material are well established at low temperatures. The sample pieces consisted of two identical optically polished disks, having the dimensions of 30 mm in diameter and 10 mm in thickness, with an apparent density 2372 Kg mm^{-3}, manufactured in Germany and supplied by LKB Beckman Instrument AB in Stockholm.

The thermal conductivity data from these measurements confirmed that the system is ready for further conductivity measurements (see Results and Discussions).

In addition to what was mentioned above about the need to obtain the valid data for fused quartz, it also meant to determine how the limits of the accuracy and

precision of the measurements are affected by several possible systematic errors that could happen during performing the experiment. Systematic errors could be due to thermal expansion, heat leaks, electrical noise from cables connecting the electronics to the device being measured (which is down inside the cryostat), noise due to electrical and magnetic fields from the power cables, etc.

The thermal conductivity curves of fused quartz are shown in Fig. 2.9 where the solid line represents the recommended values given in the literature [1,32,33], and the circles represent our measurements. The scattering of the mean values of our data in comparison to the recommended ones is within 2%. [Appendix IV].

It should be noted that the fused quartz measurements also confirm that the TPS sensors still have well defined TCR values down to liquid nitrogen temperatures, and that they can be used to determine thermal transport properties, particularly thermal conductivity values. Furthermore, all possible errors that could happen during measurements are included within the 2% deviations of the measured data from the recommended values.

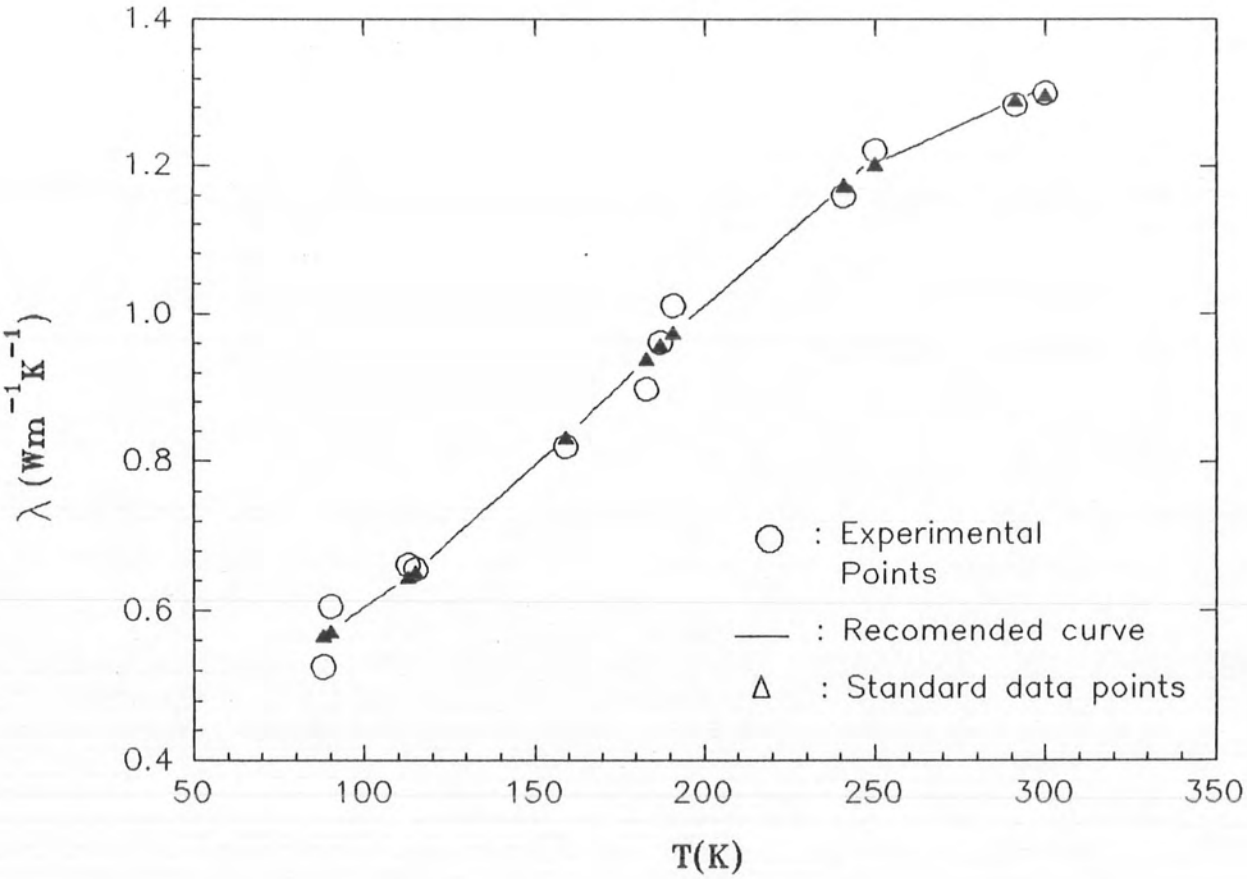

Fig. 2.9 The thermal conductivity of fused quartz versus temperature.

2.6 PREPARATION AND CHARACTERIZATION OF HIGH-T_C SUPERCONDUCTORS

SAMPLE PREPARATION

For the preparation of Y123, a solid state sintering technique was used. A description of the different steps in the preparative route of YBaCuO superconductor and the experimental set up is presented in the following section.

CHEMICALS USED

The oxides or carbonates of appropriate metals were used as a starting materials. The oxides used were Y_2O_3 and CuO with purity 99.99%. Reactant utilized in the form of carbonates was Ba CO_3 with purity 98%.

CRUCIBLE MATERIALS

Crucibles and glazed dishes made of porcelain material have been used for heating the sample because these have high melting point (1700^0C) having no reaction with the material being heated and are easily available.

MIXING AND GRINDING

The chemicals were weighed within 1mg accuracy. The oxide/carbonate mixture was intimately mixed by grinding in an agate pestle and mortar. Acetone was used as a grinding aid and the grinding time was of the order of 2-3 hours. Since the uniformity of the of the particle size may be an important consideration for some applications of the superconductors [34,35].

FURNACES

Two types of furnaces have been used in high temperature work. In their first reaction step either tube furnace (model A1017-301, Instron England having temperature range 1150^0C with temperature controller) or programmable muffle furnace (model 110, Heraeus) has been used. Final sintering step, the reaction was always performed in a tube furnace to avoid experimental difficulties in a subsequent cooling and annealing steps, as they have always been carried under controlled atmosphere.

HEAT TREATMENTS

The main importance here is to give a general description of the preparative work. The grinded material (70 gm) was a first step to calcine as loose powders in glazed porcelain dish at 900^0C in air. This heat treatment was normally lasted for 20 hours. After cooling to room temperature the black product was reground and sintered at 920^0C for 20 hours with one or several intermittent regrindings. After the last sintering step normally at 940^0C for 20 hours, the samples were left to cool in the furnace for a period of 4-5 hours, then held at a temperature of 400^0C for another 48 hours and finally permitted to cool down to room temperature. The cooling period after the last sintering step and the subsequent heat treatments were always performed in open air atmosphere.

PALLET FORMATION

After the last grinding two big pallets were made having dia (28mm) with thickness(10mm) and a small pallet having dia (13mm). These pallets were put for final sintering at 940^0C. The sample resistance at room temperature was of the order of 4-6 ohms.

CHARACTERIZATION

Polycrystalline superconductor $RBa_2Cu_3O_{7-\delta}$(R=Y,Er) was characterized by various methods such as Meissner effect, electrical resistivity, and thermal conductivity (see results and discussion).

MEISSNER EFFECT

Meissner effect is a positive test for a specimen to be a superconductor or not. When the superconducting sample is brought near the magnet a repulsion is observed. This shows that the sample under test is a superconductor above 77K. This means that current is passing through the sample without producing any voltage. The prepared sample was also checked for the Meissner effect and found to be showing very strong repulsion.

ELECTRICAL RESISTIVITY

Electrical resistance of the material is directly proportional to its length and inversely proportional to the area of cross at constant temperature.

$$R \propto \frac{L}{A}$$

$$R = \rho \frac{L}{A}$$

$$\rho = R \left(\frac{A}{L} \right)$$

where R is the resistance of the material, A is the area of cross-section, L is the length and ρ is the resistivitty of the material. But in our experiment, the temperature of the specimen does not remain constant. This shows that the resistivity no longer remains constant but varies with temperature. Thus we can write

$$\rho(T) = R(T) \frac{A}{L}$$

$$V(T) = IR(T)$$

and therefore

$$\rho(T) = \left[\frac{V(T)}{I} \frac{A}{L} \right]$$

If the length, current and area of cross-section of the sample remain constant then the voltage drop will vary with the temperature and hence resistivity of the sample indirectly vary with temperature. Resistivity as a function of temperature is very important parameter. Using this one can predict whether the specimen is a metal, insulator, semiconductor or superconductor.

For a normal metal the resistance to the flow of electrical current is caused by the scattering of the electron in the system. One source of scattering is from elementary excitation in the system such as lattice vibrations (phonons). This electron scattering is intrinsic to the material, and gives rise to the intrinsic electrical resistivity ρI. Resistance can also be caused by defects in the lattice such as impurities, grain boundaries and twin domains, which depend on the quality of the sample. The over all resistivity can usually be written as Mattheissen's rule.

$$\rho(T) = \rho I + \rho_{def}$$

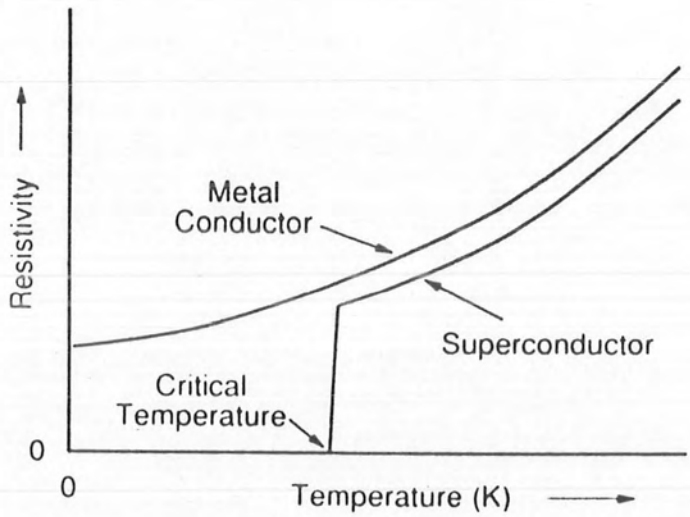

Figure 2.11 A generalized comparison of resistivity for normal metals and superconducrors as a function of temperature.

The extrinsic term ρ_{def} is typically insensitive to the temperature, while the intrinsic term ρI can be strongly temperature dependent. For example at low temperature the electron-phonon interaction yields $\rho I \propto AT^5$.

The general behavior of a normal conductor and a superconductor is shown in Fig. 2.11. The superconducting state is associated with the precipitous drop of the resistance to an immeasurable small value at a specific critical temperature T_c. Metals which are good conductors, such as Cu, Ag and Au don't become superconductor, while many poor conductors are good superconductors. The reason for the characteristically high resistivity above T_c in conventional superconductors originated from a strong electron-phonon interaction which causes the large electron scattering rate, and it is the same interaction which is responsible for the electron pairing in superconducting state. Hence a strong electron-phonon interaction produces a relatively high superconducting transition where as a weak interaction will be too feeble to produce an electron pairing. The oxide materials are also quite poor electrical conductors in the normal state, which indicates that a strong electron scattering mechanism operates in the system as well.

A number of different techniques have been applied in order to determine the electrical resistivity of metals, semiconductors, insulators, and superconductors. Which method is suitable for a specific material depends upon the form of the material i.e., whether the material under study is a single crystal, thin film, powder, or bulk polycrystalline material. In the present work the resistivity was measured by the standard four probe method[36,37]. The resistivity Vs temperature behavior is shown in Fig. 2.12. A measuring current of 10mA used for the resistivity measurement.

The crystal structure of $YBa_2Cu_3O_{7-\delta}$ as determined from neutron diffraction studies can be regarded as an oxygen-deficient supercell of an ABO_3 perovskite Fig. 2.13. The resultant orthorhombic unit cell (a=3.82$\mathring{A}$, b=3.89$\mathring{A}$, c=11.68$\mathring{A}$) consists of three cubic pervoskite blocks stacked along the crystallographic c-axis with copper atoms at the B sites; the A sites are occupied by Ba^{2+} ions in the first and third blocks and Y^{3+} in the central perovskite unit. The

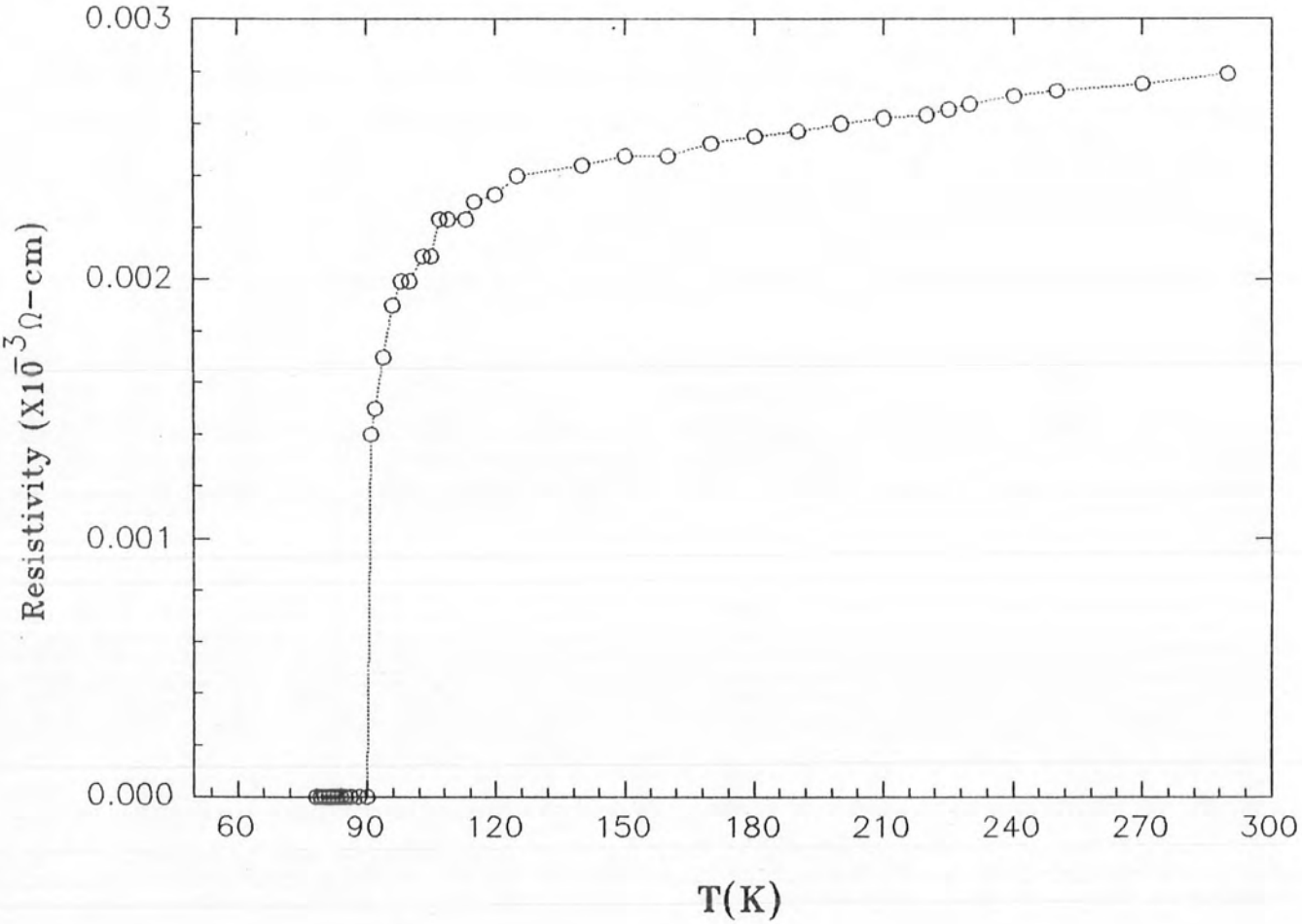

Fig. 2.12 Temperature dependence of resistivity of sample Y1.

result is the ordering of the A site cations in the sequence $Y^{3+}Ba^{2+}Ba^{2+}Y^{3+}Ba^{2+}Ba^{2+}$..... Oxygen vacancies occur on the Yttrium atom plane (at z = 1/ 2, resulting in a layered structure) and along the a axis between adjacent Cu1 atoms (at z = 0). The latter vacant sites are responsible for the orthorhombic distortion of the unit cell, since partial population of this site with oxygen atoms results in a tetragonal unit cell. Each Y^{3+} ion has square-prismatic coordination while the Ba^{2+} cations are ten-coordinated.

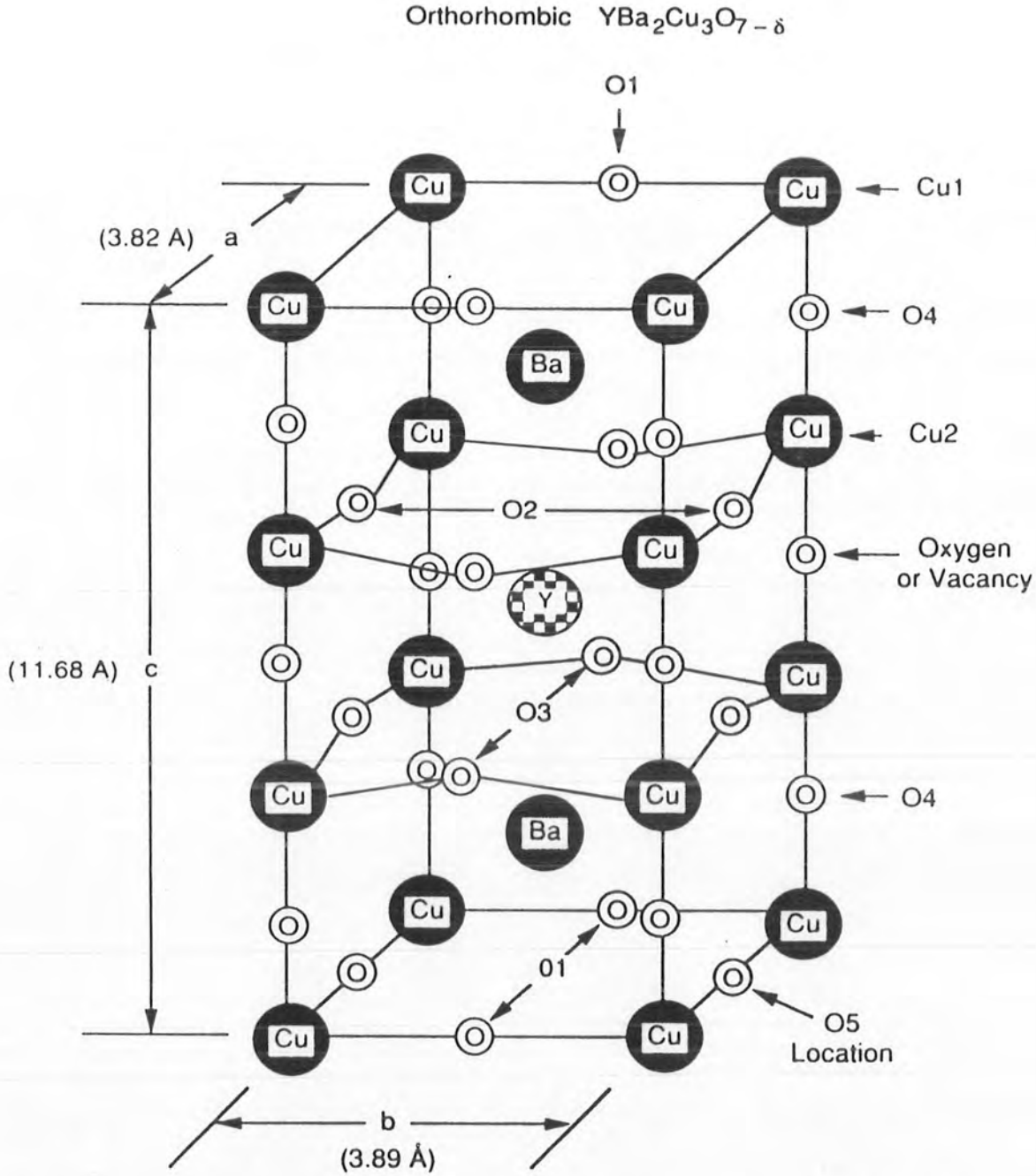

Figure 2.13 The molecular structure of the oxygen-deficient provskite unit crystal $YBa_2Cu_3O_{7-}$ [25].

CHAPTER 3

RESULTS AND DISCUSSION

RESULTS AND DISCUSSION

The advancement of technology requires the development of new materials with different ranges of thermal properties, as well as the use of these materials under severe conditions. For instance, the material used in the construction of the high pressure vessels in chemical distillation plants or in the construction of large furnaces. Furthermore, the fundamental understanding of the physical processes related to the transport of thermal energy in some of these new materials is also essential. Therefore, the development of different experimental methods to measure these properties should follow a line parallel with this progress. The reliability of a specific method is decided by several factors, such as the speed of operation, the required accuracy, the physical nature of the material, and the geometry of the available sample.

The main theme of this work was to develop an experimental setup for thermal conductivity measurements from room temperature down to liquid nitrogen temperature (77-300K). Realizing the fact that there is no one technique which is suitable for all conditions and over all temperature ranges. However, there are some techniques which can be used over quite a broad range of temperatures. One of such techniques is the recently developed Transient Plane Source (TPS), technique[29] which has been used over a temperature range from 77K up to 1000K. It has been applied for thermal conductivity measurements within the range from 0.02 up to 200 $Wm^{-1}K^{-1}$. our newly developed experimental setup provides a fair and an excellent facility for the implementation of this latest developed TPS technique.

It would be worth describing about the design criterion for the TPS-element. Waszink and Hannen [38] have demonstrated the importance of implementing a design criterion for the measurements of low thermal conductivity materials using the THS method. Their results have a direct bearing on the design criteria of the TPS-element in the sense that the conducting pattern should be laid out in such a way that the thermal conductivity is as small as possible in the radial direction from the center of the hot element (square or disk). In order to fulfill this design criterion, we need to know the thermal conductivity of the electrical insulation of the

conducting pattern (Kapton and the cement used in the production of the TPS-elements).

According to Gustafsson et al. (1986) [30], it is possible to measure the thermal conductivity of insulating layer directly, if the TPS-element is placed between two samples of high thermal conductivity, and if the effecting area of the conducting pattern is replaced by the area of the strip, as in the THS method. Using hot disc configuration with thin sheets of Kapton (total thickness upto 150μm) inserted between the hot disk and two copper blocks, the mean value of thermal conductivity is 0.13 $Wm^{-1}K^{-1}$[12]. Depending on the specific configurations, the geometry of the TPS-element determines the effective value of the thermal conductivity, which thus can depend on the direction. For the hot disk the thermal conductivity in the plane of the element is essentially constant in all directions. Using typical values e.g. 0.4 mm for the width of the nickel spiral 0.6 mm for the average distance between the spiral strips, and using the thermal conductivity value of Kapton, the effective thermal conductivity in the radial direction ($\approx$ 0.21 $Wm^{-1}K^{-1}$) is much smaller than the effective thermal conductivity in a direction to any radius of the hot disk ($\approx$ 23 $Wm^{-1}K^{-1}$). When this design criterion is satisfied, the hot disk element has been used successfully to perform measurements on materials with thermal conductivity's as low as 0.02 $Wm^{-1}K^{-1}$.

To test the validity of the experimental apparatus for conductors ,the stainless steel sample (SS 215/3) commonly known as carbon steel was studied. This sample has been selected due to their current technological and commercial importence. The chemical composition of this sample is

	%		%
C	0.91	Ni	0.038
Si	0.23	Cr	0.040
S	0.031	Cu	0.052
P	0.011	Al (Total)	0.004
Mn	0.68		

This sample had been made available through Analytical Standards AB, Swedon . The sample was in the form of circular disc of 40 mm in diameter and 18 mm in thickness. The surface of this sample was polished and made smooth so as to ensure perfect thermal contact between the sample and the heating element, as the TPS-element is sandwiched between the two discs of the material in the sample holder. The experimental arrangement for the measurement of the thermal transport properties of the stainless steel sample at the 23°C is similar as explained earlier [section 2.5] and the mean value of thermal conductivity at 23°C of this sample is 31.39 $Wm^{-1}K^{-1}$. which is well consistent as found in literature at this temperature.

The thermal conductivity λ, of $YBa_2Cu_3O_{7-\delta}$ was measured between 78 K and 298 K using the same experimental arrangement as was used for the fused quartz sample for calibration purpose. Details of the sample arrangement and different pieces of apparatus involved in these measurements are given in the section [2.5.5]. The TPS-element is used both as heat source and temperature detector. The technique is based on a three dimensional heat flow inside the sample which is regarded as an infinite medium. One of the advantage of this technique is that the temperature increase of the sample due to the current pulse does not exceed 1K even for relatively large samples thus eliminating the heat lost by radiation, and reducing the probability of the convective heat mechanism[39,40]. This mechanism has been suggested to be related to the temperature gradient across the sample and has been proposed to be adopted as an explanation of the increase of λ below T_c. The resistance measurements were performed by dc four-probe method with a measuring current of 10 mA. The size of the samples for the thermal conductivity measurements was infact the largest ever reported for this kind of measurements[41]. The samples of resistivity measurements were made from the same batch and cut from smaller pallets (10 mm diameter). The resistivity measurement are shown in Fig. 2.12. The sample shows a sharp superconducting transition. The zero resistance temperature T_c is 89 K. The onset temperature of linear behavior is around 95 K. Since the resistivity above T_c is relatively large and varies linearly with temperature, it may suggest that the scattering of charge carriers is mainly by phonons in this temperature range and the Matthiessen's rule may be used to fit the resistivity data to

a straight line. The slope of this line may be taken as an estimation of the resistivity change due to scattering by phonons.

The thermal conductivity data (Appendix III) in the vicinity of T_c is shown in Fig. 3.1. A slight deviatiopn is observed is observed around 160K for this sample which is of particular interest[15]. At T_c, there is a net change in the slope of the curve, then the thermal conductivity increases with increasing temperature above T_c and below T_c decreases slowly for this sample down to room temperature showing a higher values of λ.

To interpret the thermal conductivity behaviour around T_c in connectiion with the linearity in the electrical resistivity behaviour of the the high T_c oxides in general, one may assume the validity of of Matthiessen's rule and express the relative contributions of the carriers conduction λ_c and lattice conductiion λ_ℓ to the total thermal conductivity as

$$\lambda = \lambda_c + \lambda_\ell$$

Assuming an elastic scattering, an upper limit to the carriers thermal conductivity in the normal state can be calculated using the Wiedemann Franz law:

$$\lambda_c = L_0 T \rho^{-1}$$

where $L_0 = 2.45 \times 10^{-8} V^2 K^{-2}$

An estimation of λ_c is also shown in Fig. 3.1. It is noted that the estimated λ_c values do not exceed 9% of the total thermal conductivity in the revelant temperature range. Thus , above T_c the largest contribution to the total thermal conductivity seems to be due to lattice conduction.

The sharp upturn of the measured thermal conductivity and further increase for $T < T_c$ arises from the decrease in scattering of phonon by carriers as later condense into superconducting pairs. This will cause a faster increase of λ_ℓ which predominates the decrease in λ_c leading to a net increase in the measured thermal conductivity.

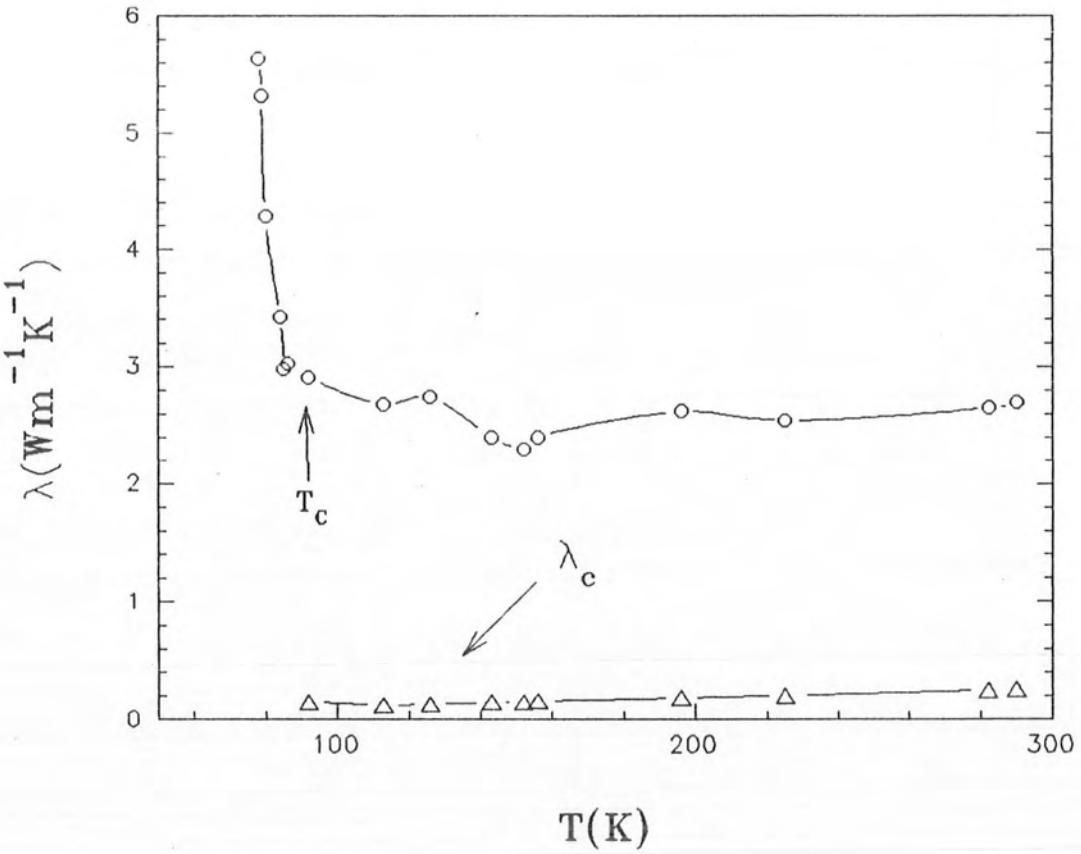

Fig. 3.1 The thermal conductivity data of $YBa_2Cu_3O_{7-\delta}$ Versus temperature, Δ represents the carrier contribution to λ as indicated by the inclined arrow, the vertical arrow indicate the corresponding T_C.

CONCLUSIONS

The TPS method has many advantages, including simplicity in operation, low cost and relatively fast. The TPS method is shown to be a convenient probe for measurements of thermal properties at low temperature, including the thermal conductivity of polycrystalline solid ceramic samples. A small temprerature increase (0.1-1K) is sufficient when relatively large size samples are studied. The corresponding temperature gradient is small (0.02-0.2 K/mm), and it becomes much easier to study the temperature dependence. This is essential when the thermal conductivity varies rapidly as for the case of superconducting samples. Also the thermal radiation from the sample boundries into the surroundings is avoided, because the transient recording is terminated before the thermal wave reaches the boundaries. By adapting the proper design of the TPS-element, the method can be used for the studies of materials within a wide range of thermal conductivity values in the temperature range from liquid nitrogen 77.36 K to 1000 K. At higher temperatures the Kapton insulation is to be replaced by a mica material.

It is also possible to calibrate these resistive-elements, as for as the TCR is concerned (the TPS sensors have well defined TCR values all the way down to liquid nitrogen temperature), prior to the experiment, and in that way it can also be used for estimating the starting temperature via R_0, which is automatically determined in a transient recording . In the TPS-technique the resistance of the hot disc is nearly twenty times the initial resistance of the hot strip in the THS technique. This actually enables us to keep the current and hence the power fed to the source at low values. Furthermore, due to the design of the TPS-element in the form of a disc, the characteristic time of the experiment is quite large as compared to the THS method.

After designing the experimental setup regarding the low temperature thermal transport studies, a simple cryostat with a dipstick was designed. The Pumping system was installed with this cryostat for vacuum purpose and all the measurements were performed in nitrogen gas flow at atmospheric pressure which was introduced via the gas flow port through vacuum valve before taking the first reading at the low temperature. The measurements on fused quartz (chosen as a standard reference

material) were performed for calibration purpose. The fused quartz measurements showed no hysteresis in either the cooling or heating modes. This have shown that for homogeneous materials that the deviation of the thermal conductivity values will not exceed 2% compared with the data (standard curve) reported in literature. A conducting steel sample commonly known as carbon steel was also studied for thermal transport properties. Measurements on high T_c sample (Y123) revealed the sensitivity of the method for probing a sudden enhancement of the thermal conductivity during phase transition.

The thermal diffusivity κ values are less accurate than the corresponding thermal conductivity. This is specially if it is necessary to use a relatively large time correction, which might lead to a reduction in the actual value of τ (2.4.2). Furthermore, for very small τ values i.e., ($0 < \tau < 0.06$), the accuracy in evaluating the integral of equation (2.1.13) is affected by the natural behavior of product of the special function involved in this equation. This also alter the stability of the results within the range of small τ values.

In addition to the measurements of λ and κ, it is in some cases possible to extend the method so that the specific heat per unit volume C can be obtained by further handling of the measured data. By combining Eq's. (2.1), and (2.1.12) with Ohms law, we can express the derivative of $\Delta E(t)$ as

$$\frac{\Delta E(t)}{\Delta(t)} = I_0 R_0 \alpha P_0 (\pi^{3/2} a\ \lambda)^{-1}\ \frac{\Delta D(\tau)}{\Delta(t)} \qquad (A)$$

By evaluating the derivative of the expression $\tau = \left[\frac{\kappa\tau}{a^2}\right]^{1/2}$ with respect to t, and using the relation

$$C = \frac{\lambda}{\kappa}$$

Eq. (A) is converted to

$$\frac{\Delta E(t)}{\Delta(t)} = I_0 R_0 \alpha P_0 (\pi^{3/2} a^3 C)^{-1} \frac{1}{2\tau} \frac{\Delta D(\tau)}{\Delta(\tau)}$$

The specific heat C can now be determined by evaluating the derivatives numerically.

Finally a few possibilities of the current work which, however, was not possible to achieve due to the lack of sophisticated cryostat with temperature controller and a multimeter for data recording much more than hundred data points and thus revealing more informations about the thermal transport properties of the materials. The work is under progress to design a controlled variable temperature insert system with the existing experimental setup to handle the above problems.

APPENDICES

APPENDIX 1

Valuesof the resistence and TCR (α) for the TPS-element as a function of temperature (77-373K)

S.No.	T(K)	R(Ω)	α(K^{-1})
1	77.0000	0.6904	0.0135
2	78.0000	0.6997	0.0133
3	79.0000	0.7091	0.0132
4	80.0000	0.7186	0.0131
5	81.0000	0.7281	0.0130
6	82.0000	0.7376	0.0129
7	83.0000	0.7472	0.0128
8	84.0000	0.7568	0.0127
9	85.0000	0.7665	0.0126
10	86.0000	0.7762	0.0125
11	87.0000	0.7859	0.0124
12	88.0000	0.7957	0.0123
13	89.0000	0.8056	0.0122
14	90.0000	0.8155	0.0121
15	91.0000	0.8254	0.0120
16	92.0000	0.8354	0.0119
17	93.0000	0.8454	0.0118
18	94.0000	0.8555	0.0117
19	95.0000	0.8656	0.0117
20	96.0000	0.8758	0.0116
21	97.0000	0.8860	0.0115
22	98.0000	0.8963	0.0114
23	99.0000	0.9066	0.0113
24	100.0000	0.9169	0.0112
25	101.0000	0.9273	0.0112
26	102.0000	0.9377	0.0111
27	103.0000	0.9482	0.0110
28	104.0000	0.9587	0.0109
29	105.0000	0.9693	0.0109
30	106.0000	0.9799	0.0108
31	107.0000	0.9906	0.0107
32	108.0000	1.0013	0.0107
33	109.0000	1.0120	0.0106
34	110.0000	1.0228	0.0105
35	111.0000	1.0337	0.0105
36	112.0000	1.0446	0.0104
37	113.0000	1.0555	0.0103
38	114.0000	1.0665	0.0103
39	115.0000	1.0775	0.0102
40	116.0000	1.0886	0.0101
41	117.0000	1.0997	0.0101
42	118.0000	1.1108	0.0100
43	119.0000	1.1220	0.0099
44	120.0000	1.1333	0.0099
45	121.0000	1.1446	0.0098
46	122.0000	1.1559	0.0098
47	123.0000	1.1673	0.0097
48	124.0000	1.1787	0.0097
49	125.0000	1.1902	0.0096
50	126.0000	1.2017	0.0095
51	127.0000	1.2133	0.0095
52	128.0000	1.2249	0.0094

S.No.	T(K)	R(Ω)	$\alpha(K^{-1})$
53	129.0000	1.2365	0.0094
54	130.0000	1.2482	0.0093
55	131.0000	1.2599	0.0093
56	132.0000	1.2717	0.0092
57	133.0000	1.2835	0.0092
58	134.0000	1.2954	0.0091
59	135.0000	1.3073	0.0091
60	136.0000	1.3193	0.0090
61	137.0000	1.3313	0.0090
62	138.0000	1.3434	0.0089
63	139.0000	1.3554	0.0089
64	140.0000	1.3676	0.0088
65	141.0000	1.3798	0.0088
66	142.0000	1.3920	0.0088
67	143.0000	1.4043	0.0087
68	144.0000	1.4166	0.0087
69	145.0000	1.4289	0.0086
70	146.0000	1.4413	0.0086
71	147.0000	1.4538	0.0085
72	148.0000	1.4663	0.0085
73	149.0000	1.4788	0.0085
74	150.0000	1.4914	0.0084
75	151.0000	1.5040	0.0084
76	152.0000	1.5167	0.0083
77	153.0000	1.5294	0.0083
78	154.0000	1.5422	0.0082
79	155.0000	1.5550	0.0082
80	156.0000	1.5678	0.0082
81	157.0000	1.5807	0.0081
82	158.0000	1.5936	0.0081
83	159.0000	1.6066	0.0081
84	160.0000	1.6196	0.0080
85	161.0000	1.6327	0.0080
86	162.0000	1.6458	0.0079
87	163.0000	1.6590	0.0079
88	164.0000	1.6722	0.0079
89	165.0000	1.6854	0.0078
90	166.0000	1.6987	0.0078
91	167.0000	1.7120	0.0078
92	168.0000	1.7254	0.0077
93	169.0000	1.7388	0.0077
94	170.0000	1.7523	0.0077
95	171.0000	1.7658	0.0076
96	172.0000	1.7793	0.0076
97	173.0000	1.7929	0.0076
98	174.0000	1.8065	0.0075
99	175.0000	1.8202	0.0075
100	176.0000	1.8339	0.0075
101	177.0000	1.8477	0.0074
102	178.0000	1.8615	0.0074
103	179.0000	1.8753	0.0074
104	180.0000	1.8892	0.0073

S.No.	T(K)	R(Ω)	$\alpha(K^{-1})$
105	181.0000	1.9032	0.0073
106	182.0000	1.9171	0.0073
107	183.0000	1.9312	0.0073
108	184.0000	1.9452	0.0072
109	185.0000	1.9593	0.0072
110	186.0000	1.9735	0.0072
111	187.0000	1.9877	0.0071
112	188.0000	2.0019	0.0071
113	189.0000	2.0162	0.0071
114	190.0000	2.0305	0.0070
115	191.0000	2.0449	0.0070
116	192.0000	2.0593	0.0070
117	193.0000	2.0737	0.0070
118	194.0000	2.0882	0.0069
119	195.0000	2.1027	0.0069
120	196.0000	2.1173	0.0069
121	197.0000	2.1319	0.0069
122	198.0000	2.1466	0.0068
123	199.0000	2.1613	0.0068
124	200.0000	2.1760	0.0068
125	201.0000	2.1908	0.0068
126	202.0000	2.2057	0.0067
127	203.0000	2.2205	0.0067
128	204.0000	2.2354	0.0067
129	205.0000	2.2504	0.0067
130	206.0000	2.2654	0.0066
131	207.0000	2.2804	0.0066
132	208.0000	2.2955	0.0066
133	209.0000	2.3106	0.0066
134	210.0000	2.3258	0.0065
135	211.0000	2.3410	0.0065
136	212.0000	2.3562	0.0065
137	213.0000	2.3715	0.0065
138	214.0000	2.3869	0.0064
139	215.0000	2.4022	0.0064
140	216.0000	2.4176	0.0064
141	217.0000	2.4331	0.0064
142	218.0000	2.4486	0.0063
143	219.0000	2.4641	0.0063
144	220.0000	2.4797	0.0063
145	221.0000	2.4953	0.0063
146	222.0000	2.5110	0.0063
147	223.0000	2.5267	0.0062
148	224.0000	2.5424	0.0062
149	225.0000	2.5582	0.0062
150	226.0000	2.5740	0.0062
151	227.0000	2.5899	0.0062
152	228.0000	2.6058	0.0061
153	229.0000	2.6217	0.0061
154	230.0000	2.6377	0.0061
155	231.0000	2.6538	0.0061
156	232.0000	2.6698	0.0061

S.No.	T(K)	R(Ω)	$\alpha(K^{-1})$
157	233.0000	2.6859	0.0060
158	234.0000	2.7021	0.0060
159	235.0000	2.7183	0.0060
160	236.0000	2.7345	0.0060
161	237.0000	2.7508	0.0060
162	238.0000	2.7671	0.0059
163	239.0000	2.7834	0.0059
164	240.0000	2.7998	0.0059
165	241.0000	2.8162	0.0059
166	242.0000	2.8327	0.0059
167	243.0000	2.8492	0.0058
168	244.0000	2.8657	0.0058
169	245.0000	2.8823	0.0058
170	246.0000	2.8990	0.0058
171	247.0000	2.9156	0.0058
172	248.0000	2.9323	0.0057
173	249.0000	2.9491	0.0057
174	250.0000	2.9658	0.0057
175	251.0000	2.9827	0.0057
176	252.0000	2.9995	0.0057
177	253.0000	3.0164	0.0057
178	254.0000	3.0334	0.0056
179	255.0000	3.0503	0.0056
180	256.0000	3.0674	0.0056
181	257.0000	3.0844	0.0056
182	258.0000	3.1015	0.0056
183	259.0000	3.1186	0.0056
184	260.0000	3.1358	0.0055
185	261.0000	3.1530	0.0055
186	262.0000	3.1703	0.0055
187	263.0000	3.1876	0.0055
188	264.0000	3.2049	0.0055
189	265.0000	3.2222	0.0055
190	266.0000	3.2396	0.0054
191	267.0000	3.2571	0.0054
192	268.0000	3.2746	0.0054
193	269.0000	3.2921	0.0054
194	270.0000	3.3096	0.0054
195	271.0000	3.3272	0.0054
196	272.0000	3.3448	0.0054
197	273.0000	3.3625	0.0053
198	274.0000	3.3802	0.0053
199	275.0000	3.3979	0.0053
200	276.0000	3.4157	0.0053
201	277.0000	3.4335	0.0053
202	278.0000	3.4514	0.0053
203	279.0000	3.4693	0.0052
204	280.0000	3.4872	0.0052
205	281.0000	3.5052	0.0052
206	282.0000	3.5231	0.0052
207	283.0000	3.5412	0.0052
208	284.0000	3.5593	0.0052

S.No.	T(K)	R(Ω)	$\alpha(K^{-1})$
209	285.0000	3.5774	0.0052
210	286.0000	3.5955	0.0051
211	287.0000	3.6137	0.0051
212	288.0000	3.6319	0.0051
213	289.0000	3.6502	0.0051
214	290.0000	3.6684	0.0051
215	291.0000	3.6868	0.0051
216	292.0000	3.7051	0.0051
217	293.0000	3.7235	0.0050
218	294.0000	3.7420	0.0050
219	295.0000	3.7604	0.0050
220	296.0000	3.7789	0.0050
221	297.0000	3.7975	0.0050
222	298.0000	3.8161	0.0050
223	299.0000	3.8347	0.0050
224	300.0000	3.8533	0.0050
225	301.0000	3.8720	0.0049
226	302.0000	3.8907	0.0049
227	303.0000	3.9095	0.0049
228	304.0000	3.9282	0.0049
229	305.0000	3.9471	0.0049
230	306.0000	3.9659	0.0049
231	307.0000	3.9848	0.0049
232	308.0000	4.0037	0.0049
233	309.0000	4.0227	0.0048
234	310.0000	4.0417	0.0048
235	311.0000	4.0607	0.0048
236	312.0000	4.0798	0.0048
237	313.0000	4.0989	0.0048
238	314.0000	4.1180	0.0048
239	315.0000	4.1372	0.0048
240	316.0000	4.1564	0.0048
241	317.0000	4.1756	0.0047
242	318.0000	4.1949	0.0047
243	319.0000	4.2142	0.0047
244	320.0000	4.2335	0.0047
245	321.0000	4.2528	0.0047
246	322.0000	4.2722	0.0047
247	323.0000	4.2917	0.0047
248	324.0000	4.3111	0.0047
249	325.0000	4.3306	0.0047
250	326.0000	4.3502	0.0046
251	327.0000	4.3697	0.0046
252	328.0000	4.3893	0.0046
253	329.0000	4.4089	0.0046
254	330.0000	4.4286	0.0046
255	331.0000	4.4483	0.0046
256	332.0000	4.4680	0.0046
257	333.0000	4.4878	0.0046
258	334.0000	4.5076	0.0046
259	335.0000	4.5274	0.0045
260	336.0000	4.5472	0.0045

S.No.	T(K)	R(Ω)	$\alpha(K^{-1})$
261	337.0000	4.5671	0.0045
262	338.0000	4.5870	0.0045
263	339.0000	4.6070	0.0045
264	340.0000	4.6269	0.0045
265	341.0000	4.6470	0.0045
266	342.0000	4.6670	0.0045
267	343.0000	4.6871	0.0045
268	344.0000	4.7072	0.0045
269	345.0000	4.7273	0.0044
270	346.0000	4.7475	0.0044
271	347.0000	4.7677	0.0044
272	348.0000	4.7879	0.0044
273	349.0000	4.8081	0.0044
274	350.0000	4.8284	0.0044
275	351.0000	4.8487	0.0044
276	352.0000	4.8691	0.0044
277	353.0000	4.8894	0.0044
278	354.0000	4.9098	0.0044
279	355.0000	4.9303	0.0043
280	356.0000	4.9507	0.0043
281	357.0000	4.9712	0.0043
282	358.0000	4.9918	0.0043
283	359.0000	5.0123	0.0043
284	360.0000	5.0329	0.0043
285	361.0000	5.0535	0.0043
286	362.0000	5.0741	0.0043
287	363.0000	5.0948	0.0043
288	364.0000	5.1155	0.0043
289	365.0000	5.1362	0.0042
290	366.0000	5.1570	0.0042
291	367.0000	5.1778	0.0042
292	368.0000	5.1986	0.0042
293	369.0000	5.2194	0.0042
294	370.0000	5.2403	0.0042
295	371.0000	5.2612	0.0042
296	372.0000	5.2821	0.0042
297	373.0000	5.3030	0.0042

APPENDIX 2

Values of the resistance for the Pt. resistance thermometer as a function of temperature (77-300K)

S. NO.	T(K)	R(Ω)
1	77.0000	20.2200
2	78.0000	20.6500
3	79.0000	21.0800
4	80.0000	21.5100
5	81.0000	21.9400
6	82.0000	22.3700
7	83.0000	22.8000
8	84.0000	23.3200
9	85.0000	23.6600
10	86.0000	24.0900
11	87.0000	24.5200
12	88.0000	24.9400
13	89.0000	25.3700
14	90.0000	25.8000
15	91.0000	26.2300
16	92.0000	26.6500
17	93.0000	27.0800
18	94.0000	27.5000
19	95.0000	27.9300
20	96.0000	28.3500
21	97.0000	28.7800
22	98.0000	29.2000
23	99.0000	29.6300
24	100.0000	30.0500
25	101.0000	30.4700
26	102.0000	30.9000
27	103.0000	31.3200
28	104.0000	31.7400
29	105.0000	32.1600
30	106.0000	32.5900
31	107.0000	33.0100
32	108.0000	33.4300
33	109.0000	33.8500
34	110.0000	34.2700
35	111.0000	34.6900
36	112.0000	35.1100
37	113.0000	35.5300
38	114.0000	35.9500
39	115.0000	36.3100
40	120.0000	38.4600
41	125.0000	40.5500
42	130.0000	42.6300
43	135.0000	44.7000
44	140.0000	46.7600
45	145.0000	48.8200
46	150.0000	50.8800

S.No.	T(K)	R(Ω)
47	155.0000	52.9200
48	160.0000	54.9700
49	170.0000	59.0400
50	180.0000	63.0900
51	190.0000	67.1200
52	200.0000	71.1300
53	210.0000	75.1300
54	225.0000	81.1000
55	250.0000	90.9800
56	270.0000	98.8300
57	280.0000	102.7000
58	290.0000	106.6300
59	300.0000	110.5100

APPENDIX III

Thermal conductivity data of $YBa_2Cu_3O_{7-\delta}$

S.No.	T(K)	$\lambda(Wm^{-1}K^{-1})$	$\lambda_C(Wm^{-1}K^{-1})$
1	78.0000	5.6400	
2	79.0000	5.3190	
3	80.0000	4.2840	
4	84.0000	3.4200	
5	85.0000	2.9800	
6	86.0000	3.0200	
7	92.0000	2.9100	0.1503
8	113.0000	2.6800	0.1240
9	126.0000	2.7400	0.1286
10	143.0000	2.4000	0.1444
11	152.0000	2.3000	0.1505
12	156.0000	2.4000	0.1545
13	196.0000	2.6200	0.1833
14	225.0000	2.5430	0.2042
15	282.0000	2.6500	0.2468
16	290.0000	2.6950	0.2538

APPENDIX IV

Thermal conductivity data of fused quartz

S.No.	T(K)	Experimental Points	Standard Points
1	88.0000	0.5250	0.5669
2	90.0000	0.6060	0.5722
3	113.0000	0.6620	0.6452
4	115.0000	0.6560	0.6523
5	159.0000	0.8209	0.8325
6	183.0000	0.8977	0.9394
7	187.0000	0.9612	0.9572
8	191.0000	1.0110	0.9748
9	241.0000	1.1600	1.1740
10	250.0000	1.2220	1.2029
11	291.0000	1.2850	1.2909
12	300.0000	1.3000	1.2985

REFERENCES

1 J.E. Parrott and Audrey D. Stukes, " Thermal conductivity of solids ", Pion Limited., London, (1975).

2 Donald M. Ginsberg, " Physical properties of high temperature superconductors III ", World Scientific Publishing Co. Ltd., (1992).

3 k. Mendelssohn and J. Olsen, Proc. Phys. Soc. **A 63**, 2 (1950).

4 J. Bardenn, G. Rickayzen and L. Tewordt, Phys. Rev. **113**, 982(1959).

5 L. Tewordt and Th. Wolkhausen, Solid State Commun. **75**, 839 (1989).

6 R. Berman, " Thermal conduction in solids ", Clarendon Press, Oxford, (1976).

7 N. Achcroft and N Mermin, " Solid State Physics " , Holt-Saunders Japan, Ltd., Tokyo, (1976).

8 C. Kittel, " Introduction to Solid State Physics " (5th ed.), John Wiley, New York (1976).

9 J. M. Ziman, " Electrons and Phonons ", Clarendon, Oxford (1960).

10 C. Uher, J. Supercond. **3**, 337 (1990).

11 A. Junod, " Physical Properties of High Temperature Superconductors ", Vol 2 Ed. D. M. Ginsberg, World Scientific Teaneck, NJ (1990).

12 B. M. Suleiman, " Ph. D. Thesis ", Chalmers University of Technology, Sweden (1994).

13 L . Tewordt and Th. WÖlkhausen, Solid State Commun. **70**, 839(1989).

14 L . Tewordt and Th. WÖlkhausen, Solid State Commun. **75**, 515(1990).

15 A. Jezowski ; J. Mucha, K. Rogacki, R. Horyn, Z. Bukowski, M . Horobiowski, J. Rafalowski, J. Stepien- Damm, C. Sulkowski, E. Trosnar, A. J. Zaleski and J. Klamut, Phys. Lett. **A 122**, 431(1987).

16 J. L . Cohn, S. A. Wolf, T.A. Vanderah, V. Selvamnickam and K. SALAM, Physica C **192**, 435 (1992).

17 S.D. Peacor, R. A. Richardson, F. Nori and C. Uher, Phys. Rev. **B 44**, 9505(1991).

18 F. Cabannes and M.L. Minges, High Temp. — High press. **21**, 69 (1989).

37 H. D. Yang , H.C. Ku., P. Klavis and R. N. Shelton, Phys. Rev. **B 36,** 8791(1987).

38 J.H. Waszink and G.E. Hannen, " Proceeding of the 9th International Heat Transfer Conference in Jerusalem ", Vol 3, Ed. Hefsoni, 193(1990).

39 C. Can Gorter, J. Phys. **34,** 1334(1956).

40 V.L. Gunzburg, J. Supercond. **2,** 323 (1989).

41 B. M. Suleiman, I. Ul-Haq, E. Karawacki, A. Maqsood, and S.E. Gustafsson, Phys. Rev. **B 48**, 4095(1993).